Chapter 1

Introduction

1.1 Display Technology

Display technology has been progressing promptly, since the last few years of the 21st century, especially for the flat panel display, which is an interesting area for the electronics industry, nowadays. With the popularization of computer and wireless communication, multimedia application displays and mass information interchange become important parts for people, and the demand of technologies of display mass information in contents and pictures are becoming more imperative. Furthermore, the electronic display is the main element for information display and the application of flat panel display can be widely used in many fields, such as mobile phones, camera screens, computer monitors, and televisions. Based on the various applications, the electronic display includes Liquid Crystal Displays (LCDs), Plasma Display Panels (PDPs), Organic Light Emitting Diodes (OLEDs), Field Emission Displays (FEDs), and Cathode Ray Tubes (CRTs). Among all display, desired features of thin format, compact size, light weight, and high image quality can be provided by LCDs.

1.2 Liquid Crystal Displays

1.2.1 The fundamental concept of Liquid Crystal Displays

Nowadays, LCDs have become the most attractive information displays, as the developments of the various requirements of the applications desktop monitors, mobile phones, notebooks, televisions, etc.

The first generation of Liquid Crystal Displays was dynamic scattering mode displays. However, this type of display has become more or less obsolete with the advent of twisted nematic displays, except for some special applications. The difference between these two modes is purely dielectric and non-purely dielectric effect. The dynamic scattering mode is based on the principle of dielectric as well as on conductivity alignment as the rest of LC displays including twisted nematic mode are based on purely dielectric effect.

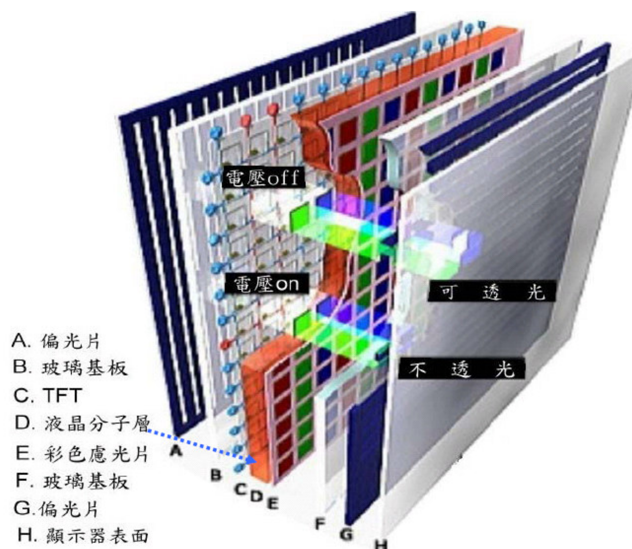

Fig. 1-1 The structure of liquid crystal display

Liquid Crystal Displays, which are passive electro-optical displays, do not generate light by itself but only modulate the light. As the development of the technology, a “transmissive type” LCD was demonstrated by Sharp Corporation in 1989 [1]. A backlight system was needed for the application of transmissive type LCD and was disposed on the rear surface. The amount of light from the backlight which transmits through the LC panel is controlled by the liquid crystal for the

purpose of displaying image. LCDs are composed of polarizer, color filter, liquid crystal, circuit plate, and backlight as shown in Fig. 1-1.

For the purpose of different kinds of applications, several types of LCDs were researched such as reflective LCD [2] and transflective LCD [3]. The transmissive type is not suitable for the outdoors display, because the ambient light is stronger than the backlight. As a result, Cholesteric liquid crystal materials which can reflect specific wavelength of light were paid great attention in the research of reflective LCDs [4]. A reflector was also utilized to reflect light recently, especially the transflective LCD used an inner reflector to reflect ambient light in reflect area, while light was displayed by backlight system in transmissive area. However, several critical issues still need to be concerned, such as achievement of full-color and simplifying the fabrication process. Compared to these types of LCDs, transmissive one is still the most promising candidate for the multimedia display application. Fig. 1-2 (a) and Fig. 1-2 (b) show the three typical structures of LCDs mentioned above.

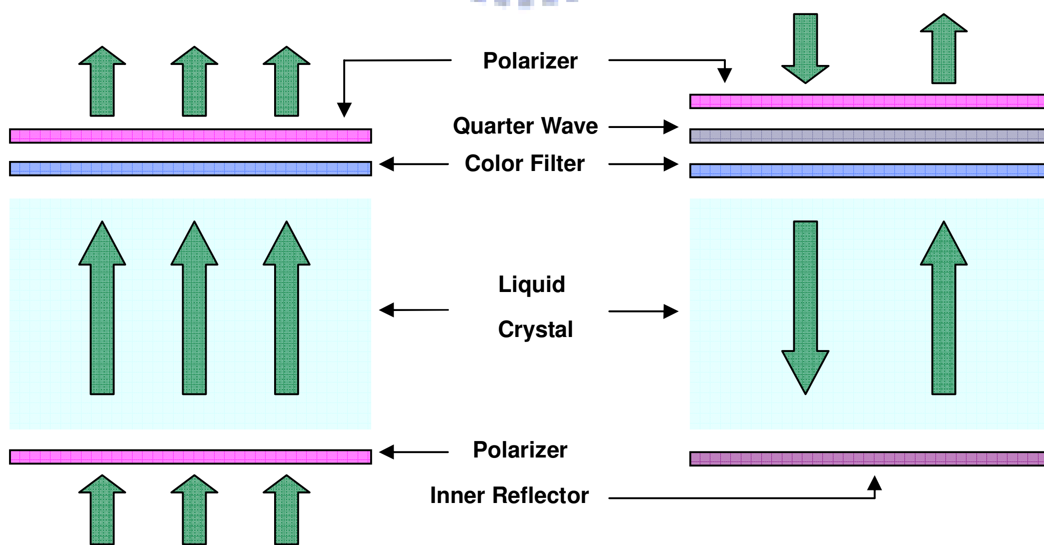

Fig. 1-2 (a) Sketch of Transmissive (left) and Reflective (Right) LCD

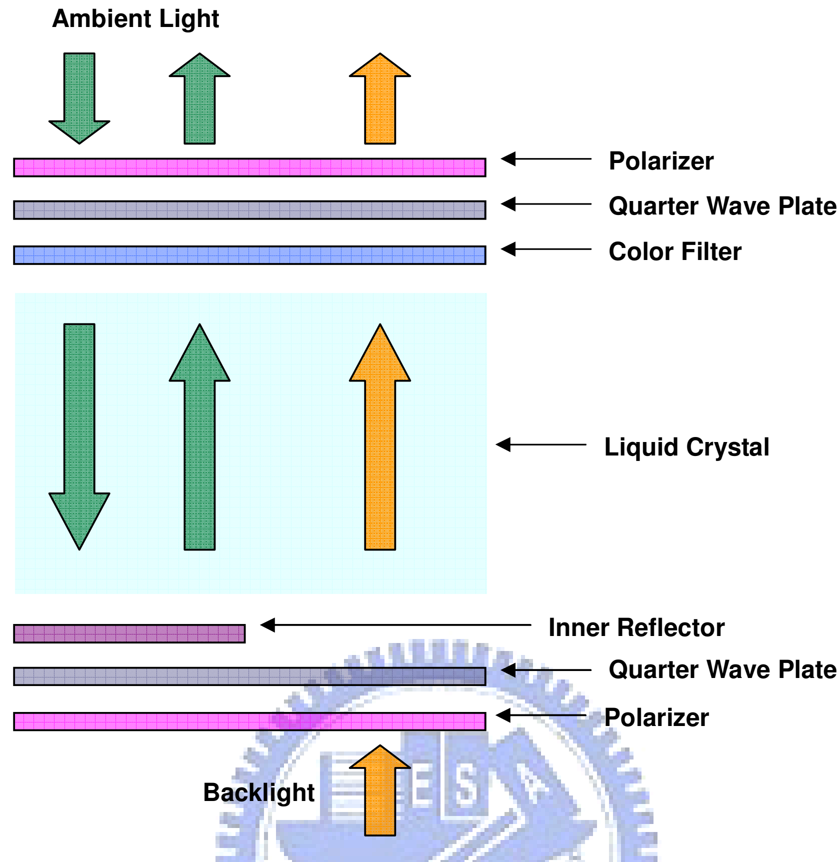

Fig. 1-2 (b) Sketch of Transflective LCD

The common LC application in transmissive LCDs is twisted nematic (TN) type. High contrast ratio and low driving voltage are its advantages; Because of the simpler and cheaper fabrication, it has been used to lots of commercial products in recent years. However, its slow response time and narrow viewing angle is viewed as the critical drawback and restrains the application of TN LCDs. In this thesis, TN mode will be used. The problem of plasma aligned TN cells will be investigated in the following chapters.

1.2.2 Operation principle of twisted nematic liquid crystal

In twisted nematic (TN) [5] liquid crystal cells, liquid crystal of positive permittivity is used. The operation principle of TN cell is shown as Fig. 1-3. The TN cell is placed between two crossed polarizers. The alignment directions of the two alignment layers are the same with the transmission axes of neighboring polarizers, with homogeneous alignment. The liquid crystal in the cell is twisted 90 degree from one substrate to another. When no voltage is applied, the polarization of incident light will rotate following the director of liquid crystal. After passing through whole cell, the polarization will rotate 90 degree and transmit the analyzer. When a voltage is applied increasingly, the liquid crystal is aligned from homogeneous to homeotropic gradually. As the voltage is larger enough, the liquid crystal molecules except the ones near the substrates are aligned perpendicular to the substrate. The polarization of the incident light will no longer rotate, and block by the analyzer.

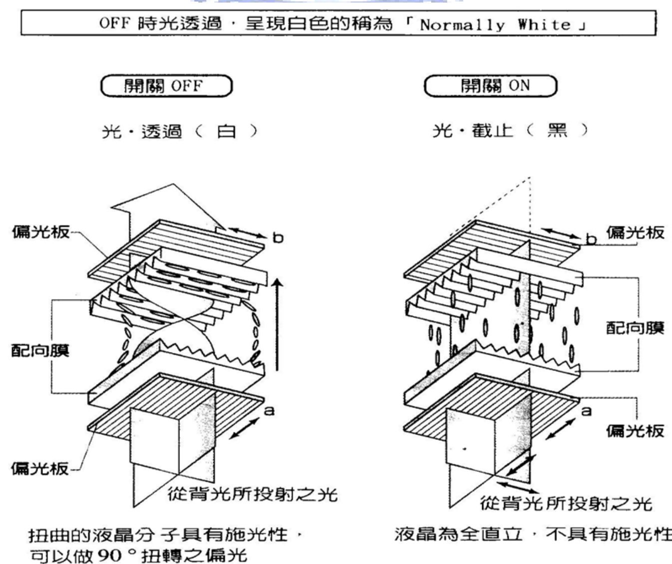

Fig. 1-3 The operation principle of twisted nematic LCD

1.3 Alignment process

Rubbing method has been adopted for alignment technologies attributed to its simple, convenient and low-cost from the early stages of LCD production in the 70s. However, while the production of TFT-LCDs started in the 80s, defects of the rubbing method were taken into account. The surface of polyimide layers is rubbed with a cloth during the rubbing procedure and several problems appeared. Static electricity, which caused by the friction between the surface of the cloth and the polyimide layers, is a critical drawback and destroys the thin film transistors (TFTs). Furthermore, Defects and stains on the surface of the alignment layer arisen from the direct contact between the surfaces and the cloth are also serious problems and restrict the development for the high definition larger sizes LCDs in the next generation.

In view of the problems mentioned above, the developments of new methods for liquid crystal alignment have been researched to take place of the conventional rubbing procedure. As a result, non-contact alignment technique had been paid into attention, such as photo-alignment and plasma beam alignment [6-10]. Photo-alignment has been a focus of research since Gibbons el al. reported their photo-alignment results in 1991 [11]. In 1994, it was found that polyimide exposed to linearly polarized deep UV light showed LC alignment, and that a wider variety of materials could be used for photo-alignment [12]. At that time, viewing angle was a critical issue to be improved and multiple domain technique adopted photo-alignment technique was investigated to enhance the viewing angle attributed to its sample establishment of multiple domains. However, color shift problem cannot be addressed by multi-domain technique and that is the reason why photo-alignment did not become widespread as a mass production line. Recently, not only linearly polarized

light, but also non-polarized light can be selected as the light source for the photo-alignment [13~14]. Furthermore, the relatively weak anchoring energy and non-stability by photo-alignment technique compared to the rubbing process is still a challenge to be overcome. The main progress and trends to the photo-alignment technique are summarized in Fig. 1-4. The requirements for the light sources for photo-alignment are almost the same as those for lithography except for the polarization state. In addition, high energy density light sources which can generate linearly polarized light for larger exposure area have been investigated recently.

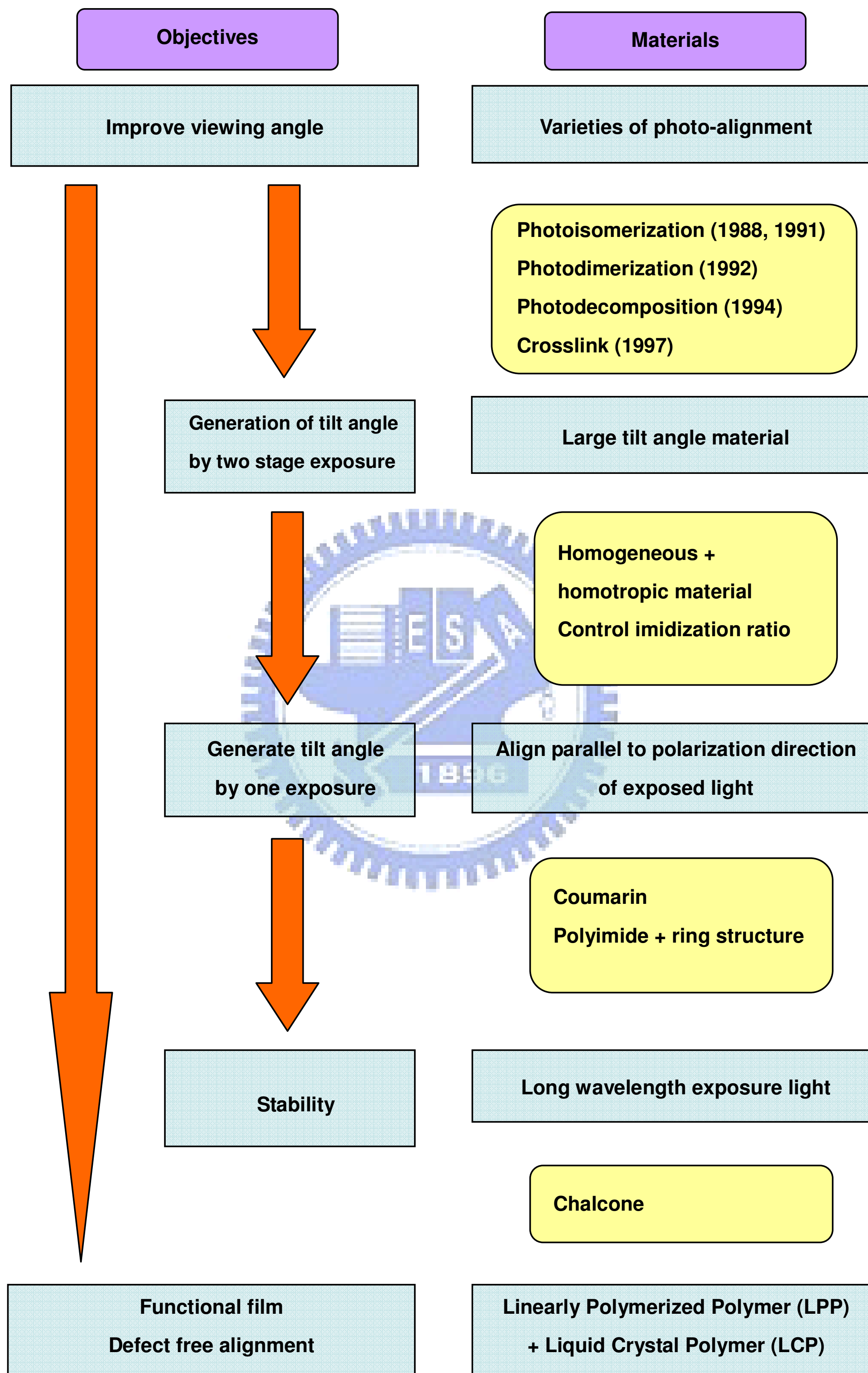

Fig. 1-4 History of the development of photo-alignment

Since photo-alignment still has some critical drawback, ALT plasma alignment technique is our solution because of its relatively higher anchoring energy and stability than that with photo-alignment. The basic construction and theory of the ALT plasma alignment technique will be described in Chapter 2 in detail.

1.4 Motivation and Objective

The conventional rubbing process is used to align the alignment layer for a long time. However, the alignment layer is contacted directly by the cloth and induces some drawbacks, such as debris and electrostatic charge. The drawback restricts the development of LCD production, especially for the larger size panel in the next generation.

As a result, ALT plasma alignment technique, which do not has the disadvantages of rubbing method mentioned above, was adopted for the TN mode instead of rubbing process. The electric-optical characteristics of TN cell, pretilt angle dependence, and surface roughness after plasma alignment process was obtained and discussed in detail. The problem caused by plasma alignment for TN cell was also investigated and improved in the following chapters.

1.5 Organization of This Thesis

The thesis is organized as following: The fundamental principle of ALT plasma source and alignment mechanism is presented in **Chapter 2**. After that, in **Chapter 3**, the ALT plasma alignment procedure will be introduced in detail, and the measurement instruments used to investigate the electro-optic characteristics of TN

cells, pretilt angle, surface roughness, chemical bonding structure and anchoring energy such as electro-optic measuring system, TBA, AFM and NEXAFS, will also be described. The experimental results and discussion, including the electro-optic performance of TN cells, pretilt angle dependence, surface morphology, anchoring energy and the change of chemical bonding structure after the treatment of ALT plasma, will be discussed in **Chapter 4**. Finally, the conclusions of this thesis will be presented in **Chapter 5**.

Chapter 2

Principle

2.1 Introduction

Anode layer thruster (ALT) plasma system was selected as the alignment technique in this study. The fundamental concept of this technique will be described in detail in this chapter, such as history, background, theory, operation principles and the application for the LC alignment. Moreover, the alignment mechanism of this non-contact alignment technique and previous researches will be introduced.

2.2 Discharge Characteristics

2.2.1 Plasma

Generally, the term "plasma" is used to describe a partially or completely ionized gas containing electrons, ions and neutrals. Although there is always a small degree of ionization in any gas, a stricter definition of the plasma is a "quasi-neutral gas of charged and neutral particles which exhibits collective behavior". Quasi neutrality refers to the characteristic that positive and negative space charges balance in a given volume such that the overall plasma is considered to be electrically neutral. The collective behavior of the plasma is result from the Coulomb forces that are long range and cause remote regions to interact with one another.

Micro-plasma show a new class of the plasma whose properties fall somewhere between those of glow discharge and arcs as shown in Fig. 2-1. These two types of

processing plasma are characterized to low-pressure glow discharges and high-pressure arcs. However, the low electron temperature and non-equilibrium make them more similar to glow discharges. As a result, they are often referred to as a "high pressure glow discharges".

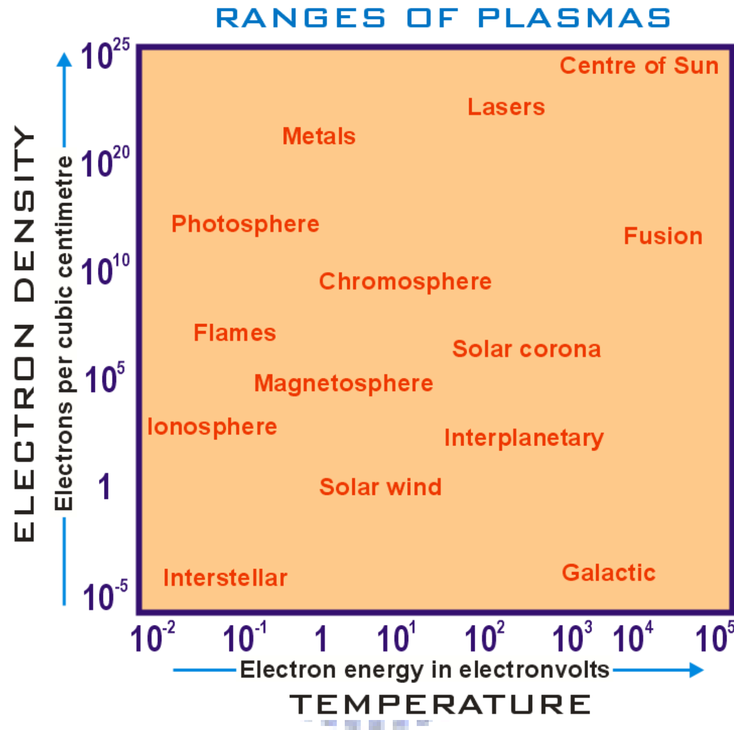

Fig. 2-1 Space and laboratory plasmas classified by their electron temperature and charged particle density

2.2.1 Glow Discharge

The name of glow discharge is the phenomenon that plasma is luminous and depends on the geometry of the electrodes and the vessel, the gas used, the electrode material. Furthermore, the phenomenon of gas breakdown is considered as the

transition from insulating state to conducting state. The associated voltage required to cause the transition is referred to as the breakdown voltage. Current flows between the electrodes via the movement of charged particles (ions and electrons) to and from the electrodes. When the electrons are energetic enough to dissociate the gas through impact to create ions, formation of a gas discharge occurs. The average electron temperature, T_e, is generally less than breakdown energy required for ionization.

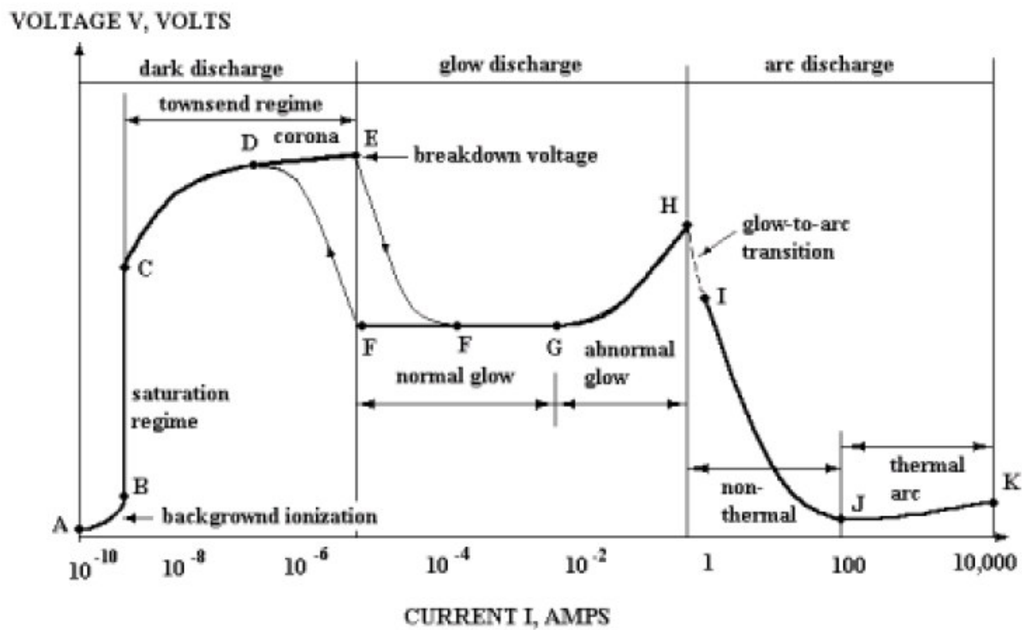

Fig. 2-2 Voltage-Current (V-I) characteristic for a discharge

When breakdown occurs, the gas suddenly becomes conductive. The current and voltage in the gas discharge vary resulting changing supply voltage. These parameters can be investigated to obtain a voltage-current (V-I) characteristic for a discharge as illustrated in Fig. 2-2. Moreover, current is limited through the discharge by using an external ballast resistor.

Three general regions can be identified on the diagram above, the dark discharge (Townsend region), the glow discharge and the arc discharge. Because the discharge remains invisible to the eye except for corona discharge and the breakdown itself, the regime between A and E on the voltage-current characteristic is termed a dark discharge. The electric field sweeps out the ions and electrons created by ionization from background radiation during the *background ionization*. The ions and electrons migrate to the electrodes in the applied electric field producing a weak electric current. Increasing voltage results in an increasing fraction of these ions and electrons. If the voltage between the electrodes is increased far enough, eventually all the available electrons and ions are swept away, and the current saturates. The region is named the saturation region because the current remain constant while the voltage is increased. After the voltage across the *saturation region*, the current will rise exponentially. The electric field is now high enough so the electrons initially present in the gas can acquire enough energy before reaching the anode to ionize a neutral atom. As the electric field becomes even stronger, the secondary electron may also ionize another neutral atom leading to an avalanche of electron and ion production. The region of exponentially increasing current is called the *Townsend discharge*. The *Corona discharge* occurs in the region of *Townsend discharge* because of high electric field near sharp points, edges, or wires in gases prior to electrical breakdown. If the coronal currents are high enough, *corona discharge* can be technically “glow discharges”, visible to the eye. For low currents, the entire corona is dark, as appropriate for the dark discharge. After the breakdown, the gas enters the *normal glow* region, which the voltage is almost independent of the current over several orders of magnitude in the discharge current. The electrode current density is independent of the total current in this region. This means that the plasma is in contact with only a small part of the cathode surface at low currents. As the current is increased, the fraction of the cathode

occupied by the plasma increased until plasma covers the entire cathode surface. For the next *abnormal glow* region, the voltage increases significantly with the increasing total current in order to force the cathode current density above its natural value and provide the desired current. The third general region is arc discharge. The electrodes become sufficiently hot that the cathode emits electrons thermo-ionically. If the DC power supply has a sufficiently low internal resistance, the discharge will undergo a glow-to-arc transition. The *arc regime*, from I through K is one where the discharge voltage decreases as the current increases, until large currents are achieved at point J, and after that the voltage increases slowly as the current increases.

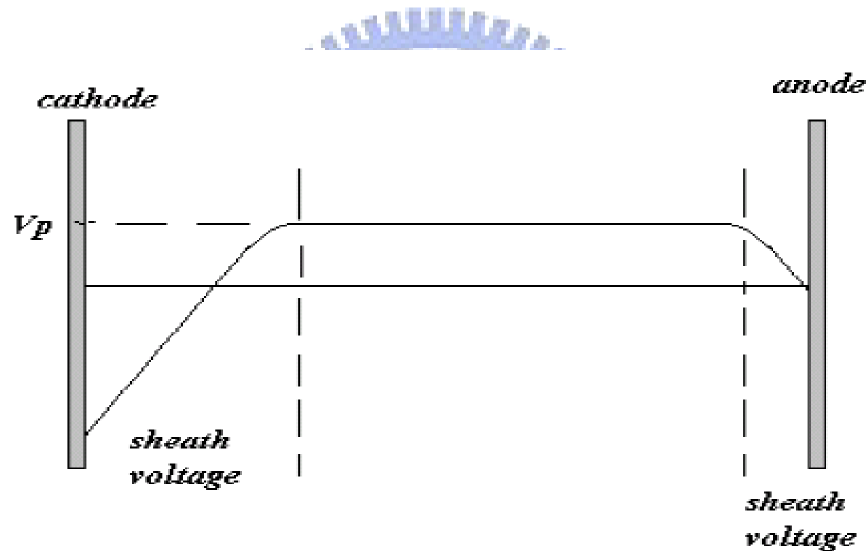

Fig. 2-3 Voltage distribution in a dc glow discharge process

Besides, the glow discharge owes its name to the fact that plasma is luminous. The glow can be produced by applying a potential difference between two electrodes in a gas. The potential drops rapidly close to the cathode, vary slowly in the plasma, and change again close to the anode. Fig. 2-3 shows the voltage distribution in a dc glow discharge process. The electric fields in the system are restricted to sheaths at each of the electrodes. The sheath fields are such as to repel electrons trying to reach

either electrode. Electrons originating at the cathode will be accelerated, collide, transfer energy, leave by diffusion and recombination, slow by the anode and get transferred into the outside circuit. The luminous glow is produced because the electrons have enough energy to generate visible light by excitation collisions. Since there is a continuous loss of electrons, there must be an equal degree of ionization going on to maintain the steady state. The energy is being continuously transferred out of the discharge and hence the energy balance must be satisfied also. Simplistically, the electrons absorb energy from the field, accelerate, ionize some atoms, and the process becomes continuous. Additional electrons are produced by secondary emission from the cathode. These are very important to maintaining a sustainable discharge.

2.3 Anode Layer Thruster (ALT) Source

2.3.1 History and Background

There has been a growing interest in recent years in ion beam surface treatment technology to meet the demands for improved surface properties of base materials for electronics and optical devices in terms of adhesion, hardness, electrical resistance and chemical stability. In order to apply the surface modification in an industrial scale, a number of requirements should be met. For example, large area irradiation, long lifetime, reliable and stable performance of the ion source. Many researches had paid attention to the ion sources with small irradiation areas. In addition, Hall thrusters, also called closed drift thrusters (CDT), have been used for the satellite propulsion in Russia during the past 30 years and was the strong candidate for the ion sources application with the large irradiation area. Two main modern variants can be classified for the closed drift thrusters as shown in Fig. 2-4. One is anode layer thruster (ALT)

and the other is stationary plasma thruster (SPT). The name "closed drift" means azimuthal drift of electrons that is general to all family of such thrusters. Stationary plasma thruster (SPT) has the extended acceleration zone compared with the anode layer thruster (ALT) and normally used for the insulator chamber walls. Notwithstanding the two have differentiating features in their operation and performance, they base on the same fundamental principles for ionizing and accelerating the propellant. These principles were first correctly optimized experimentally through the seminal work of Janes and Lowder (1965). [15]

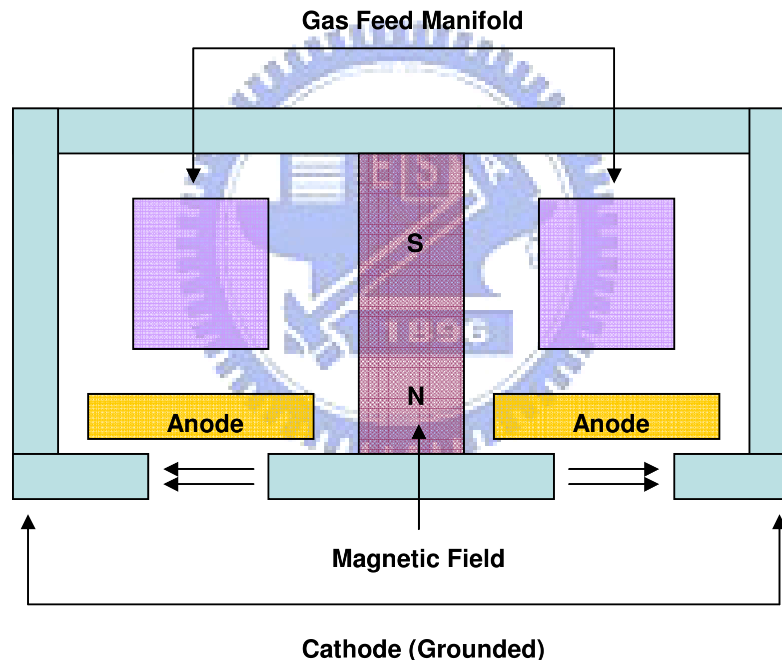

Fig. 2-4 Cross-sectional schematic drawing of the linear ion source

The plasma irradiation is generated by anode layer thruster (ALT). Fig. 2-5 shows the schematic diagram of the ALT system. The ALT source consists of outer and inner cathode and anode. Permanent magnet is necessary to generate magnet pole at outer cathode. The plasma flux is generated by cross electric field (E) and magnetic

field (H) immediately. In ALT source, several operating parameters can be selected, such as incidence, energy and manufacturing gases. The gases chosen to proceed alignment process will affect the properties of alignment layer.

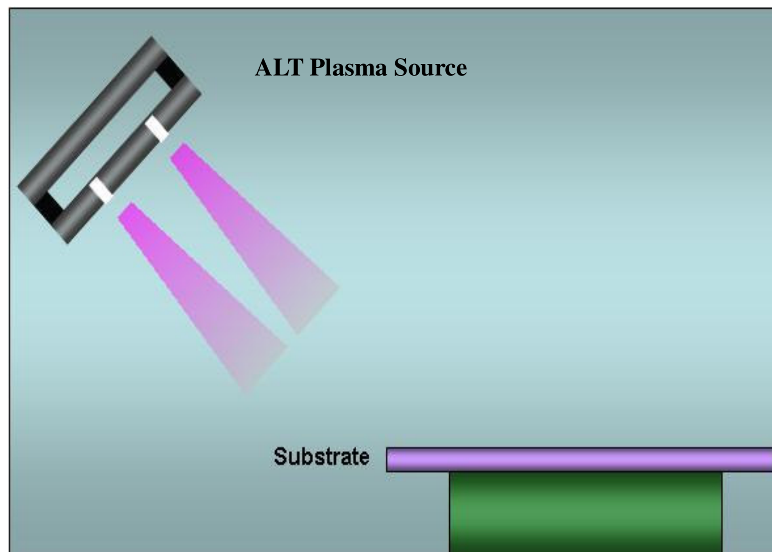

Fig. 2-5 Schematic diagram of ALT plasma system

1896

2.3.2 Application for LC Alignment

Liquid Crystal Display is the most popular device and is indispensable to our daily life. To achieve high performance, alignment layers which control the liquid crystals molecular orientation are the most critical part in any current LCDs. The function of alignment layer inside the cell is to align LC toward desired direction and pretilt angle. It should be highly uniform with desirable alignment parameters, such as selective pretilt angle and strong anchoring energy and plays a very important role to influence the electro-optical performance of the LCD. Among many alignment method, rubbing is the widely used process attributed to the simple construction and low cost. However, it is widely recognized and inevitable some existing drawbacks of

the rubbing procedure. Debris and electrostatic charge are the common disadvantages of the rubbing and have the serious limitation for the development of the LCD, especially for the high resolution and the large size. The development of new alignment process is necessary to vanquish intrinsic problems of rubbing process mentioned above. Among many possible candidates for the alignment methods, plasma beam methods are especially attractive.

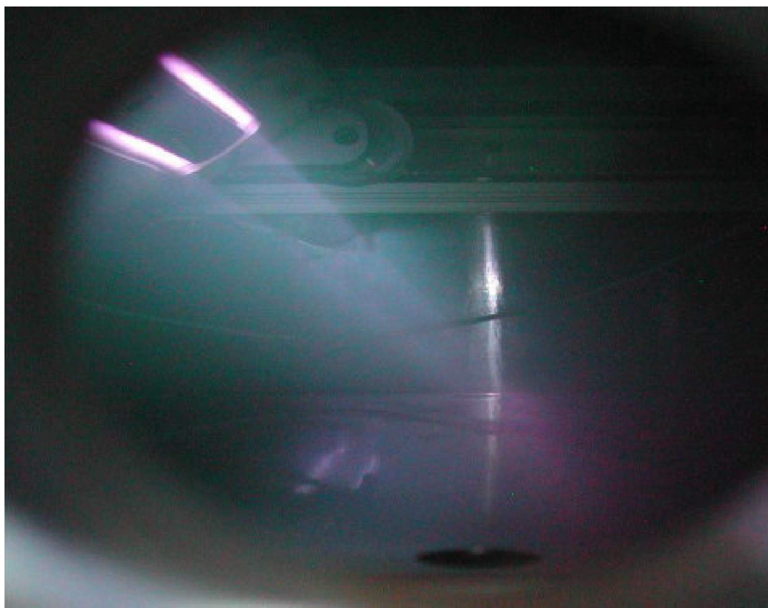

Fig. 2-6 ALT Plasma beam with race-trap shape

In this experiment, plasma beam alignment technique has been developed for large scale non-contact mode alignment method. The flux of plasma beam obliquely treats on the surface of the alignment substrate and result in the anisotropic property on the alignment surface. Z. M. Sun etl., investigated on the molecular orientation of nematic 5CB on various solid substrates sputtered by an Ar^+ ion beam experimentally in 1994 and is the first research on the LC orientation by this method. [16] Since IBM group studied the organic and inorganic films by atomic beam alignment and

demonstrate the 13.3 inch prototype laptop computer. [17~18] Their idea is based on the treatment with low ion energy and only very top layer of the alignment surface is influenced. Plasma beam alignment has been paid great attention to take the place of the conventional rubbing process. Fig. 2-6 shows the ALT plasma beam with race-trap shape in the chamber. As a result, ALT plasma alignment used in this experiment is the promising technique to substitute for the traditional rubbing method for the next generation.

2.3 Alignment Mechanism

With many disadvantages of associated with mechanical rubbing, non-contact alignment of liquid crystals has the most promising substitution for this conventional method. As a result, plasma alignment was the selection by ALT plasma source in this experiment. Moreover, the alignment mechanism of this non-contact technique had been studied for a long period. Previous studies indicate that bond scission and cross-linking are the major processes on argon ion beam interaction with polymers. Several factors influence the plasma beam bombardment, such as the plasma energy and the chemical structures of the polymers [19~20]. J. Stohr et al. suggested that orientational order is created by preferential bond breaking and bond formation relative to ion beam direction by using near edge X-ray absorption spectroscopy (NEXAFS) [21]. In addition, X-ray photoelectron spectroscopy (XPS) is usually used simultaneously because NEXAFS does not provide information on the chemical changes produced in the alignment layer during the ion beam bombardment. As a result, polarized attenuated total reflection infrared spectroscopy (ATR-IR) is the better selection because it can provide orientational and chemical information of the polymer surface, which is directly related to the alignment mechanism. J. E. Fulghum

et al. investigated the alignment mechanism of the polyimide (PI 2555) with the instrument, ATR-IR, and suggest that selective destruction of the weakest bonds (π bonds) in the polymer by the argon ion beam result in a net excess of the remaining π bonds, which cause the anisotropy in these π bonds align liquid crystals parallel to the ion beam propagation direction [22].

Chapter 3

Fabrication and Measurement Instruments

3.1 Introduction

New approach adopted ALT plasma alignment technique for TN mode cells were proposed in this thesis. The fabrication process and measurement instruments will be also described in this chapter. The fabrication sequences of the proposed method included the substrate, ALT plasma alignment procedure and the cell formulation. The commercial available indium-tin oxide (ITO) glass was cleaned by standard process in advance. Afterwards, the ITO surface was irradiated by UV-Ozone for 30 minutes and then spins coating, a semiconductor process, was utilizing in order to acquire the uniform alignment layer. After the spin coating process, the alignment surface was treated by the ALT plasma source with controllable parameters. The cell fabrication puts together the ITO substrates with accurate alignment. The cell gap was controlled approximately 25 μm by spacers and the space between the two ITO substrates was filled with the nematic LC (Merck ZOC-2293) for TN. After cell process, the pretilt angle and electro-optical performance of the TN cell were investigated.

Moreover, the surface morphology and chemical information of alignment surface after ALT plasma treatment was investigated by atomic force microscope (AFM) and near-edge x-ray absorption fine structure (NEXAFS) spectroscopy. The major features of the instruments mentioned above will be described in detail in this chapter.

3.2 Fabrication Process

3.2.1 Flow chart

The flow chart of the fabrication process of the TN cells was illustrated as following and provides the overview of the whole cell fabrication process as shown in Fig. 3.1. The ITO glass cleaning, spin coating with polyimide, ALT plasma alignment and cell formulation will be described in detail in the next section.

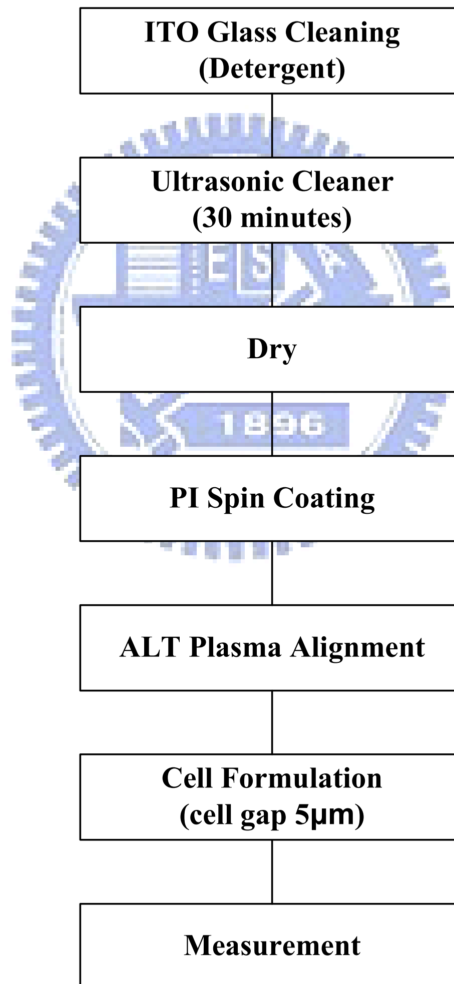

Fig. 3-1 The fabrication flow chart of the TN cell

3.2.2 Cell Fabrication

(a) Substrate cleaning

The glass was widely used as a substrate for the display application area. As a result, the glass substrate cleaning plays a very important role to influence the display. In the fabrication, the glass of about 1.1 mm thick was selected and ITO was uniformly sputtered on the glass. The ITO glass was firstly cleaned by detergent and then deionized water in an ultrasonic cleaner for 30 minutes and then dried by nitrogen gas. Afterwards, the ITO glass was backed on the hot plate with the temperature, 100°C, for 30 minutes.

(b) Spin coating

After the ITO substrate cleaning, the ITO surface was firstly exposed by the UV-Ozone for 20 minutes. The polyimide (Chisso 5580-01A) was selected and mixed with the solvent (Chisso NBG-667) before spin coating. Right after that, polyimide thin film was spin-coated upon the ITO layer with the lower spin-rate, 800 rpm, for 20 sec and the higher spin-rate, 5000 rpm, for 60 sec. Afterwards, the polyimide thin film was baked on the hot plate at the temperature, 200°C, for 1 hour.

(c) ALT plasma alignment

Throughout the previous two processes, ALT plasma alignment upon the spin-coated polyimide layer is the following step. At the beginning, the inside pressure was pumped to the base pressure, 2×10^{-4} torr. Afterwards, several

parameters can be controlled during the plasma alignment, such as incident angle, gas, exposure time and voltage. In this experiment, the incidence of the plasma beam source was fixed at 70° and the sample was scanned by the ALT plasma source. Investigating the influence of the alignment surface and electro-optic performance of the TN cell is our concern. During the plasma alignment process, the gases were introduced into the chamber, such as Ar, H_2 and O_2 with 20 sccm flow rate and the working pressure was 1.25 x 10^{-3} torr. In addition, the voltage was controlled by 450 V. Table. 3-1 reveals the selected parameters of the ALT plasma alignment and the operation procedure of this alignment is also listed in Table. 3-2.

Table. 3-1 The parameters of the ALT plasma alignment

Mode	Mode 1 (Scan mode)
Voltage	450 V
Incident angle	70°
Working pressure	0.2 mtorr
Working gas 1	Ar
Gas flow rate	20 sccm
Scan times	5
Scan velocity	6 mm/s
Working gas 2	H_2
Gas flow rate	20 sccm
Scan times	1
Scan velocity	5 mm/s

Table. 3-2 The procedure of the ALT plasma alignment

Alignment Steps	
1. Incidence mode	Select the desirable one
2. Bump to Vacuum	Base pressure 2 x 10^{-4} Torr
3. Parameters Setting	Gas flow rates, exposure time
4. Plasma treatment	Working pressure 1.25 x 10^{-3} Torr

(d) Cell formulation

Two ITO Glasses were pasted crossed with twin adhesive spacers. The thickness of spacer with 25 μm is required for maintaining the cell gap. Finally, the space between two substrates was filled with the nematic LC (Merck ZOC-2293).

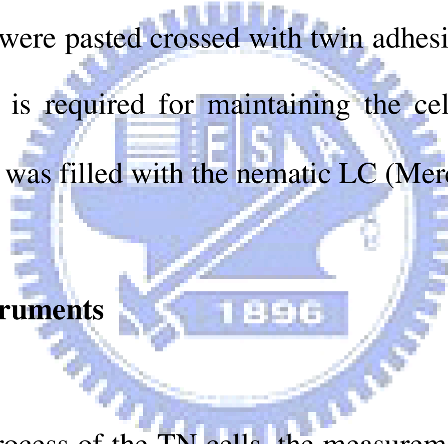

3.3 Measurement Instruments

After the whole process of the TN cells, the measurement procedure was started as following, such as pretilt angle, surface roughness, V-T characteristic and chemical bond information.

3.3.1 Electro-optical Measurement System

The electro-optical measurement system is shown in Fig. 3-2. This optical system is responsible for the measurement of V-T characteristics. In the beginning, the intensity of laser source within the acceptable range of the photo detector is needed to be reduced by using a 10% ND filter. As following, the moderate unpolarized light

becomes a polarized light after passing through the polarizer and then enters the LC cell. The LC cell, acted as a phase modulator, changes the phase of the incident polarized light by retardation $\Delta n \cdot d$ (Δn is the birefringence of LC, and d is the thickness of LC). After that, the modulated light passes through the analyzer and the light output is received by the photo detector. The driving waveform was sent by a waveform generator WFG500 (from FLC Electronics AB). The V-T curve is measured by using a 1k Hz bipolar square wave. The optical output received by the photo detector can be observed with the oscilloscope (from Tektronix) and quantified data can be read by a multimeter (from Keithley).

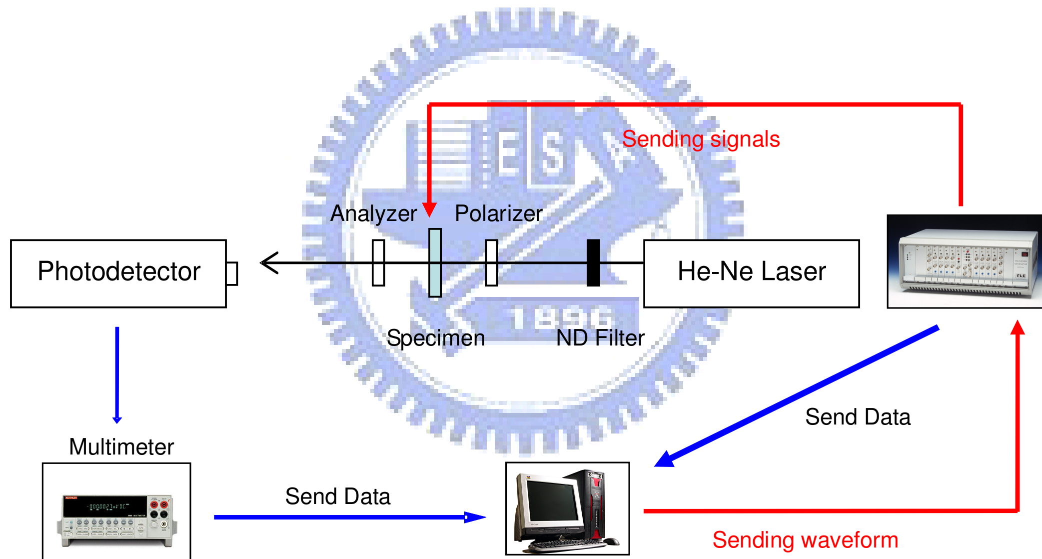

Fig. 3-2 The schematic diagram of electro-optical measurement system

3.3.2 Cell Gap Measurement System

For liquid crystal display, the thickness of cell gap usually affects the optical performance. As a result, the cell gap measurement has to be understood in advance as the following procedure of the measurement. The measurement instrument used is UV/Vis spectrometer LAMBDA 950 from Perkin Elmer, and the principle of this method is introduced as below.

The basic concept of the measurement method is based on the interference of light reflected by the two reflecting surfaces. [23-24] The illustration is as Fig. 3-3. R1, a coefficient of reflection, is defined as ratio of the light reflected by surface 1 to the incident light. R2 is the reflection coefficient of surface 2.

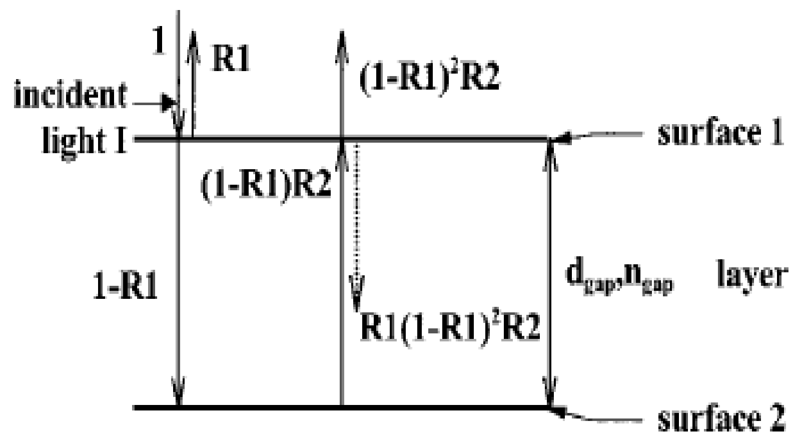

Fig. 3-3 Two reflecting surfaces separated by a layer causing a light interference

The dotted line indicates the first internal reflection

If the total incident light is $I = \cos \omega t$ and there is no any absorption of light in surface 1and 2 was assumed, then we can write the total reflected light R as

$$R = R_1 \cos\omega t + \sum_{k=1}^{\infty} R_1^{\,k-1} R_2^{\,k} (1-R_1)^{1+k} \cos\omega(t-kt_o) \qquad (3\text{-}1)$$

Where $\omega = 2\pi c n_{gap}^{\frac{1}{2}}/\lambda$ and $t_0 = 2d_{gap} n_{gap}^{\frac{1}{2}}/c$, c is the speed of light in the vacuum, λ is the wavelength, d_{gap} is the thickness of the layer, n_{gap} is the refractive index of the layer. The cosine factor in Eq. (3-1) for k>1 are caused by internal reflections. Since R1<1 and R2<1, the magnitude of the cosine factors for k>1 is much smaller than for k=1. Therefore the internal reflection is chosen to be neglected, so

$$R = R_1 \cos\omega t + (1-R_1)^2 R_2 \cos\left(\omega t - \frac{4\pi n_{gap} d_{gap}}{\lambda}\right) \qquad (3\text{-}2)$$

Thus the reflected spectrum is

$$|R(\lambda)|^2 = R_1^{\,2} + \left[(1-R_1)^2 R_2\right]^2 + 2R_1(1-R_1)^2 R_2 \times \cos(4\pi n_{gap} d_{gap}/\lambda) \qquad (3\text{-}3)$$

The periodic term in Eq.(3-3) causes an interference pattern. The periodicity of the reflected interference spectrum determined the optical thickness of the cell gap, $n_{gap} d_{gap}$.

If λ_1 and λ_2 are the two wavelengths showing extrema in Eq.(3-3), then $\cos(4\pi n_{gap} d_{gap}/\lambda) = \pm 1$ for $\lambda = \lambda_1$ and $\lambda = \lambda_2$. Therefore

$$2n_{gap} d_{gap} = k_1 \lambda_1 / 2 \qquad (3\text{-}4)$$

$$2n_{gap} d_{gap} = k_2 \lambda_2 / 2 \qquad (3\text{-}5)$$

Where k_1 and k_2 are natural numbers. Suppose $\lambda_1 > \lambda_2$, then

$$k_2 = k_1 + x \tag{3-6}$$

Where x is a natural number.

Based on Eqs.(3-4), (3-5), and (3-6), we can write

$$n_{gap} d_{gap} = \frac{x \lambda_1 \lambda_2}{4(\lambda_1 - \lambda_2)} \tag{3-7}$$

The value of x-1 indicates the number of extrema in $|R(\lambda)|^2$ between the wavelengths λ_1 and λ_2. It is better to choose the distance x between the two extrema as large as possible for improving the accuracy of the calculation of $n_{gap} d_{gap}$. The sample data was shown in Fig. 3-4 for a 5.0 µm cell.

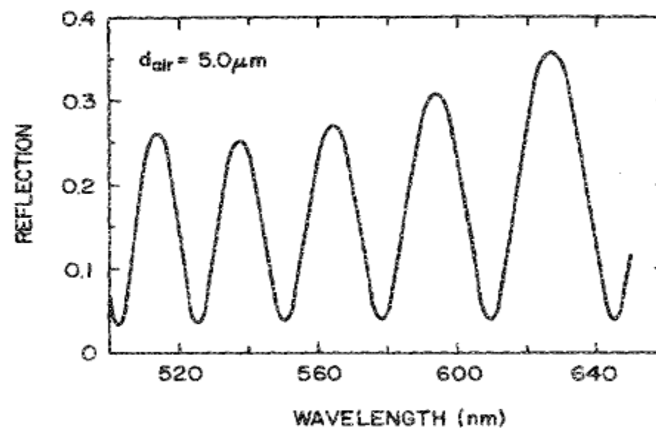

Fig. 3-4 The reflection as a function of wavelength using a air gap of 5.0µm

3.3.3 Pretilt Angle Measurement System

Fig. 3-5 Pretilt angle measurement system (Autronic DMS 101 TBA)

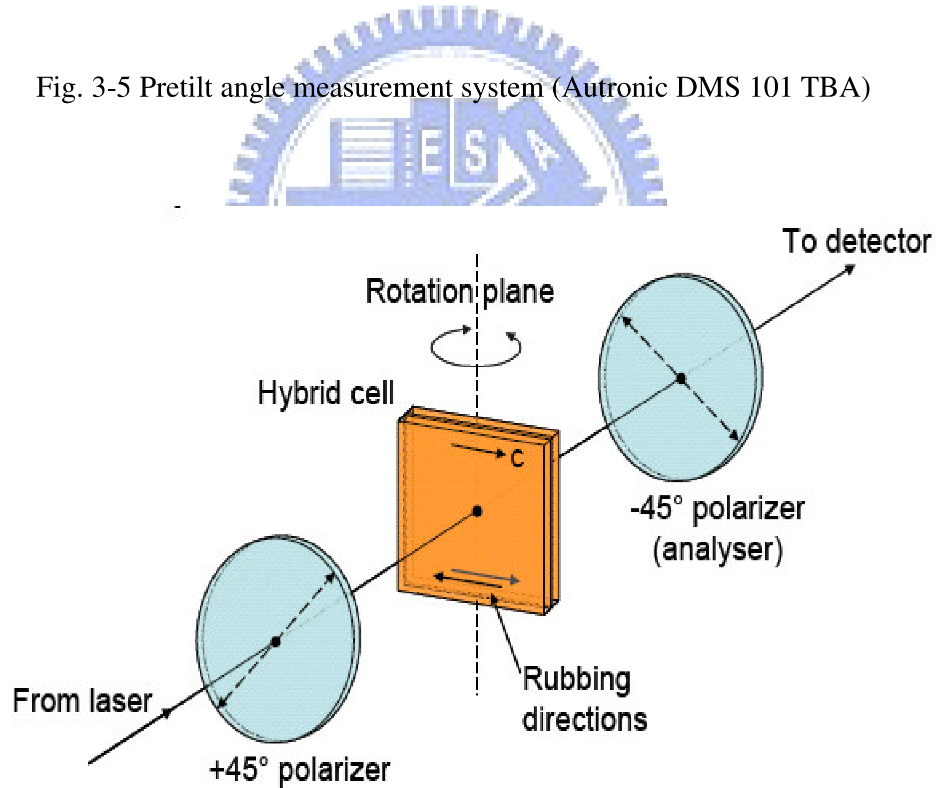

Fig. 3-6 Schematic diagram of crystal rotation method

An anti-parallel symmetric cell was assembled to measure the pretilt angle with the crystal rotation method [25] (Autronic DMS 101 TBA instrument) as shown in Fig.

3-5. The cell was rotated with rotation stage while the transmitted laser power through the analyzer was measured. He-Ne laser with the wavelength 632.8 nm is the laser source. Stepper driven rotary stage with 2x10-3 degree resolution can measure from planar to homeotropic (0-90 degrees) and cell gap from 20-60um. The schematic diagram of crystal rotation method is shown in Fig. 3-6.

3.3.4 Atomic Force Microscopy (AFM)

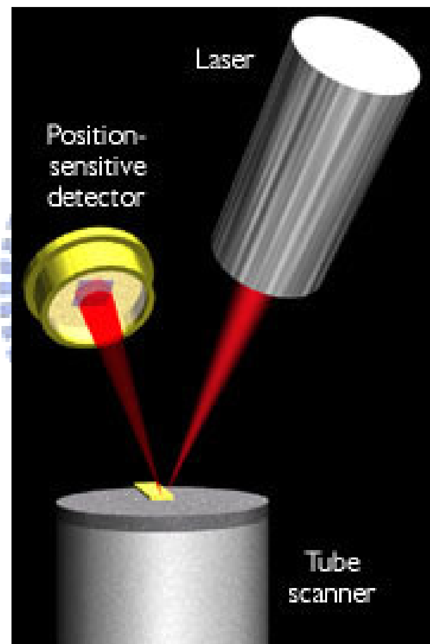

Fig. 3-7 Concept of AFM and the optical lever

Atomic Force Microscope (AFM) [26] consists of a sharp tip mounted on the end of a flexible cantilever spring. Forces from the sample act on the tip and generate some measurable change in the cantilever, such as deflection or shift in resonant frequency. To form an image, the interaction between the sample and tip is mapped to the monitor as a function of position mechanically scanning the sample relative to the

tip in a raster pattern into the photo-detector. By detecting the difference in the photo-detector output voltages, changes in the cantilever deflection or oscillation amplitude are determined. A schematic diagram of this mechanism is depicted in Fig 3-7.

There are two major operation modes for AFM:

(a) Contact mode

Contact mode is the most common method to operate the AFM. As the term suggests, the tip and the sample remain in close contact as the scanning proceeds. One of the drawbacks of remaining in contact with the sample is that there exists a large lateral force on the sample as the tip is dragged on the specimen.

(b) Taping mode

Tapping mode consists of oscillating the cantilever at its resonance frequency (typically hundreds of kilohertz) and positioned above the surface so that it only taps the surface for a very small fraction of its oscillation period. The laser deflection method is used to detect the root-mean-square (RMS) amplitude of cantilever oscillation. The advantage of tapping mode over contact mode is that it eliminates the lateral, shear forces present in contact mode, which enables tapping mode to image soft, fragile, and adhesive surfaces without damaging them.

3.3.5 Near-Edge X-ray Absorption Fine Structure (NEXAFS) Spectroscopy

In order to observe the surface property of nano-scale substances, many spectral-analytic technologies related to X-ray are always applied, such as X-ray

photoelectron spectroscopy, near edge X-ray absorption spectroscopy, X-ray emission spectroscopy, etc. Using these analytic technologies can figure out the properties of electrons nearby atoms in a matter, which provide direct and complete information of material bonding characteristics. Among these technologies, Near Edge X-Ray Absorption Fine Structure (NEXAFS) [27-29] spectroscopy has been applied in the research of liquid crystal alignment in recent years. [21,30-31]

NEXAFS is element-specific due to the different energy of absorption edge for different element, as Fig. 3-8. NEXAFS has high sensitivity for the bonding environment of absorbed atoms because of the fine structure near each absorption edge, and always concentrates on the region within about 30~50 eV of the absorption edge. Moreover, these fine structures vary with different position and the surroundings of absorbed atom, as shown in Fig. 3-9. Obviously, NEXAFS has the ability of partial chemical bonding environmental identification.

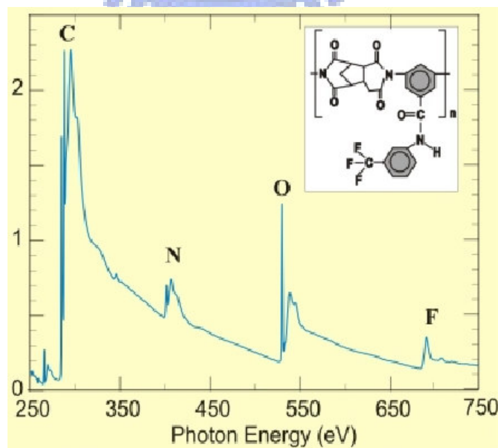

Fig. 3-8 NEXAFS spectrum of different element

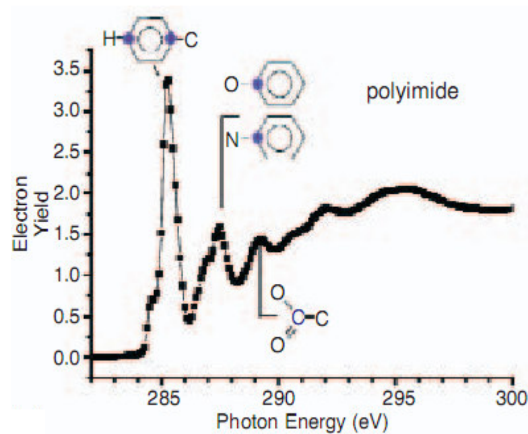

Fig. 3-9 Near edge X-ray absorption fine structure spectrum (carbon K-edge)

Linear polarized X-ray is chosen as the excited light source in NEXAFS. The absorption intensity is enhanced when the X-ray polarization is parallel to the orbital of chemical bond. The intensity of absorption is proportional to the amount of the specific chemical bonding. By changing incident angle and the direction of polarization, the information of directional chemical bonding can be obtained.

NEXAFS (Near Edge X-ray Absorption Fine Structure) spectroscopy is one of operation modes of photoelectron emission microscopy (PEEM). [27-29] The sampling depth in total electron yield mode is a few nanometers, while in the Auger electron yield mode is smaller than one nanometer. The principle of NEXAFS is involved the excitation of core electrons, as shown in Fig 3-10, and the details are described in ref [28].

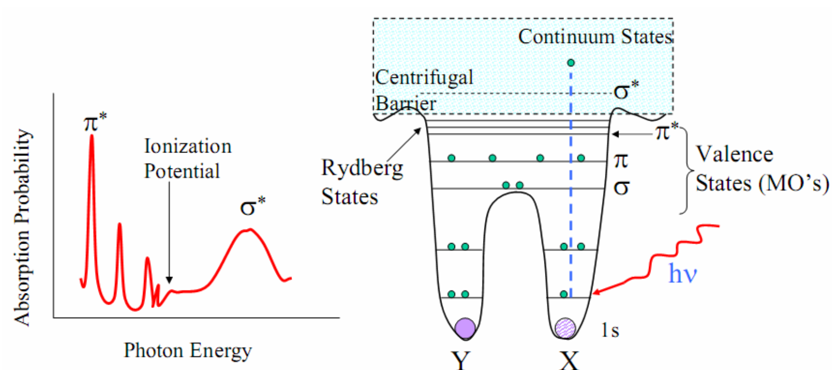

Fig. 3-10 The electron energy level of bi-molecule system, and the corresponding NEXAFS spectrum

In this thesis, the near-edge X-ray absorption fine structure (NEXAFS) spectra were taken at the X-ray photoemission electron microscopy (X-PEEM) station at the National Synchrotron Radiation Research Center (NSRRC), Hsinchu, Taiwan. The s- and p-polarized radiation with an energy resolution of 100 meV at the carbon K-edge was delivered to the sample at a 65° incident angle. Both the in-plane and out-of-plane chemical information of rubbing and plasma alignment will be investigated in the following chapter.

3.3.6 Anchoring Energy Measurement

Anchoring energy is usually used to describe the interaction between liquid crystal molecules and the alignment layer, and it is an important factor in liquid crystal alignment. We can use anchoring energy to quantify the alignment strength and estimate the feasibility of different alignment method. Anchoring energy can be separated into two parts: polar anchoring energy and azimuthal anchoring energy. The strength of polar anchoring energy will affect the EO properties and the tilt angle of

liquid crystal, while the strength of azimuthal anchoring energy will affect the orientational order and the alignment of liquid crystal in azimuthal direction. In this thesis, we focus on the polar anchoring energy, and connect with electro-optic characteristics of plasma and rubbing alignment.

Many methods were proposed to measure polar anchoring energy, such as surface disclination method, Freedericksz transition method [32-33], and high electric field method. [34-35] Generally, the polar anchoring strength is larger than azimuthal anchoring energy, so it is difficult to measure. In recent, the most popular method for measuring polar anchoring energy is high electric field method proposed by H. Yokoyama and H. A. Van Sprang in 1985. [34]

Consider a cell filled with positive dielectric anisotropy LC and is aligned anti-parallel. When no electric field is applied, all LC molecules are aligned parallel to the alignment direction on the substrate. When the applied voltage is larger than threshold voltage, LC molecules begin to rotate. Due to the effect of anchoring strength of two alignment layers, the rotation angle of LC molecules near the surface is smaller than the one of LC in the middle of the cell. Therefore, we can observe the optical properties of LC cell in electric field to obtain polar anchoring energy.

Based on the elastic continuum theory, the relationship between applied voltage, capacitance, and optical retardation can be simplified as follow:

$$\frac{R}{R_0} = \frac{\xi}{CV} I(\alpha, \gamma, \nu, 0) - \frac{2K_{11}}{W_{polar} d} \qquad (3\text{-}8)$$

$$R_0 = \frac{2\pi}{\lambda}(n_e - n_o)d\,, \quad \xi = (\varepsilon_{//} A/d)\pi(K_{11}/\Delta\varepsilon)^{1/2}$$

$I(\alpha,\gamma,\nu,0)$ is an integrated value related to some LC parameters:

$$I(\alpha,\gamma,\nu,0)=\frac{2}{\pi}\int_0^{\frac{\pi}{2}}\frac{1-\nu+(1-\nu)^{1/2}}{1-\nu\cos^2\delta+(1-\nu\cos^2\delta)^{1/2}}(1+\gamma\sin^2\delta)^{1/2}(1-\alpha\cos^2\delta)^{1/2}\cos\delta d\delta$$

$$\alpha=\Delta\varepsilon/\varepsilon_{//}\ ,\ \ \gamma=(K_{33}-K_{11})/K_{11}\ ,\ \ \nu=(n_e^2-n_o^2)/n_e^2 \qquad (3\text{-}9)$$

From Eq. (3-8), if we want to obtain polar anchoring energy, we must know the relation between applied voltage, capacitance, and retardation. When the applied voltage is high enough, LC molecules are almost perpendicular to the substrate, so the capacitance of the cell will almost the same with increasing applied voltage. The capacitance of the cell is seen as a fixed value at high voltage region. In Eq. 3-8, R_0 is the optical retardation of LC cell without applying voltage when LC molecules are lie on the substrate. Actually, LC molecules always have pretilt angle on the substrate, so R_0 must be corrected as $R_0^{'}$:

$$R=\frac{2\pi}{\lambda}\Delta nd\Rightarrow R_0^{'}=\frac{2\pi}{\lambda}\Delta n_{eff}(\theta)d \qquad (3\text{-}10)$$

Using these approach mentioned above, Eq. (3-8) can be rewritten as follow:

$$R=\frac{I_0}{V}-\frac{4\pi}{\lambda}\Delta n_{eff}(\theta)d_e \qquad (3\text{-}11)$$

$$I_0=\frac{\xi R_0^{'}I(\alpha,\gamma,\nu,0)}{C_a},\ \ d_e=\frac{K_{11}\sin^2\theta+K_{33}\cos^2\theta}{W_{polar}}$$

If we find the relationship between retardation and applied voltage, we can use Eq. (3-11) to obtain polar anchoring energy of the cell. The Soliel-Babinet Compensator is used in our laser system to measure the retardation of LC cells.

Another simple method for determination of polar anchoring energy by capacitance measurement had been proposed. [36] The capacitance of LC cell is determined by cell gap d, area of electrodes S and the dielectric permittivity of LC ε,

which is a function of the applied voltage. For the high voltage region $V > 6V_{th}$, the capacitance of LC cell can be written as follow: [35,37]

$$C = \frac{\varepsilon_0 \varepsilon_{//} S}{Qd}\left(1 - \frac{\overline{V}}{V}\right) \tag{3-12}$$

where $\overline{V} = \alpha \frac{\varepsilon_a}{\varepsilon_{//}} V_{th}$, $\varepsilon_a = \varepsilon_{//} - \varepsilon_{\perp}$, $V_{th} = \pi \sqrt{\frac{K_{11}}{\varepsilon_0 \varepsilon_a}}$, $\alpha = \frac{1}{\pi} \int_{y_p}^{1} \sqrt{\frac{(1+\gamma)(1+ky)}{y(1+\gamma y)}} dy$,

$$\gamma = \frac{(\varepsilon_{//} - \varepsilon_{\perp})}{\varepsilon_{\perp}},\ k = \frac{K_{33} - K_{11}}{K_{11}},\ y = \sin^2\theta,\ y_p = \sin^2\theta_p$$

$\varepsilon_{//}$, $\varepsilon_{\perp}$ is the dielectric constant parallel and perpendicular to the LC director. θ_p is pretilt angle. K_{11}, K_{33} is the elastic constant of splay and bend.

$$Q = 1 - \frac{2K_{11}}{Wd} \frac{\gamma(1+ky_p)(1-y_p)}{1+\gamma y_p} \tag{3-13}$$

For the small pretilt angle θ_p:

$$Q = 1 - \frac{2\gamma K_{11}}{Wd} \tag{3-14}$$

From Eq. (3-14) we can find the polar anchoring energy W. Measure the value of capacitance $C_{\inf}$ at high voltage limit $V \to \infty$, the value of threshold voltage V_{th} and using Eq. (3-12) we will get:

$$W = \frac{2}{\pi^2} \frac{V_{th}^2}{S} \frac{(C_{//} - C_{\perp})^2}{C_{\perp}} \frac{1}{1 - C_{//}/C_{\inf}} \tag{3-15}$$

Where $C_{\perp}$ is the capacitance of LC cell for planar orientation, $C_{//}$ is the capacitance for vertical alignment.

Both of high electric field method and capacitance measurement were used for measuring polar anchoring energy in this thesis. The comparison of these two methods will be shown in the following chapter.

Chapter 4

Experimental Results and Discussions

4.1 Introduction

The procedure of the TN cell adopted ALT plasma alignment technique was introduced in previous chapter. In order to find out the mechanism of plasma alignment, the surface morphology and the pretilt angle dependence of the alignment layer after plasma beam treatment measured by TBA and AFM will be described. The problem in V-T characteristic caused by plasma alignment will also be investigated in this chapter. The NEXAFS spectra will show the in-plane and out-of-plane chemical information after plasma treatment. New plasma alignment process is proposed to improve the dark state of V-T curve of original plasma-aligned TN cell.

4.2 Alignment Properties of Plasma Alignment

4.2.1 AFM Analysis

Surface morphology of the surface of the polyimide is an important factor, since the LC molecule directly attaches the surface. Because plasma alignment involves ion bombardment, the etching effect occurred on the alignment layer during alignment process is our concern. The scan mode was used for plasma alignment process in this thesis. Fig. 4-1 shows the surface morphology of the polyimide for different incident angle of sheet-like plasma. The incident angle is defined as the angle between the direction of plasma and the surface normal. Fig. 4-1 (a) and (b) indicate that the incident angle is 10° and 70°.

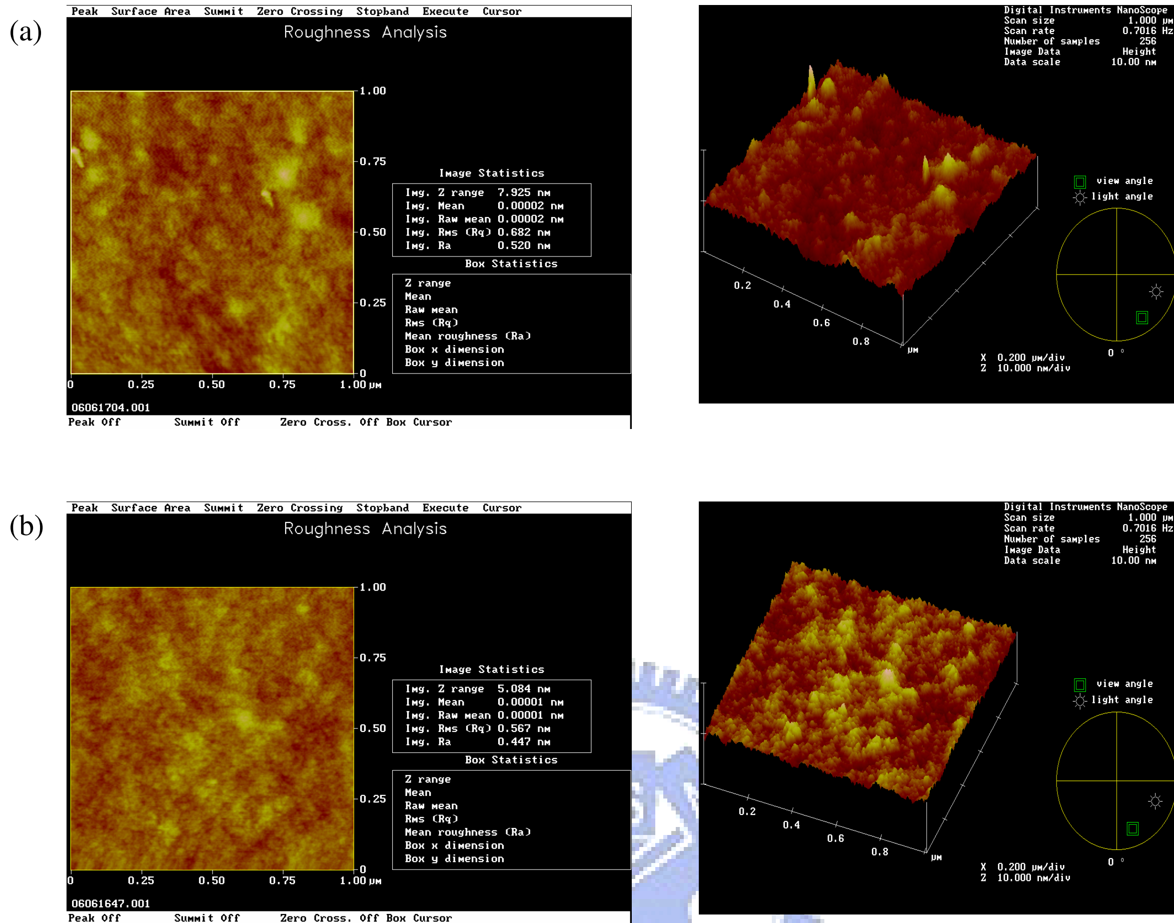

Fig. 4-1 Surface morphology of the polyimide for incident angle of (a) 10° (b) 70°

In Fig. 4-1, we found that the surface of 10° incidence is rougher than the one of 70° incidence. Because when the incident angle was 10°, the plasma was almost perpendicularly incident to the alignment layer. This case led the plasma strike the alignment layer deeper and made the etching effect clearer than high incident angle.

Next, we changed the scan times of alignment process and observed the surface morphology by using AFM. The surface morphology of the polyimide surface for different scan times is shown below. Fig. 4-2 (a), (b), and (c) indicate the surface morphology of polyimide after sheet-like plasma scan one time, five times, and ten times, respectively.

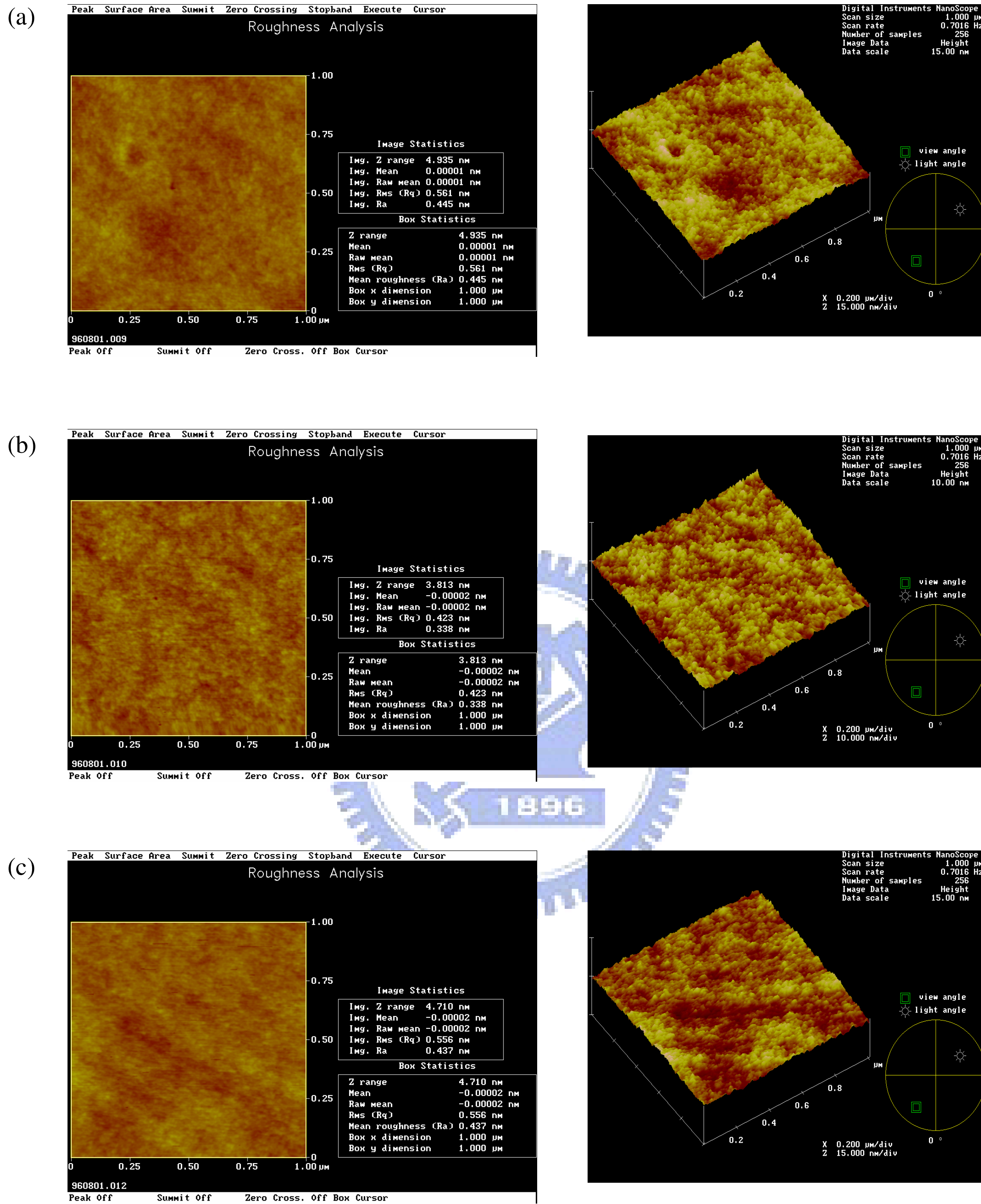

Fig. 4-2 Surface morphology of polyimide for different plasma scan times

(a) one time (b) five times (c) ten times

Since the alignment layer is bombarded by plasma continuously when the alignment process proceeds, the etching effect became more severe with increasing scan times. We can see this phenomenon in Fig. 4-2. From these AFM observations, we found that no matter what incident angle or scan times of plasma is, the surface morphology of alignment layer does not have any “directional” deformation. All we can see is the “isotropic” etching on the alignment layer. Because liquid crystals are well-aligned on the plasma treated alignment layer of isotropic morphology, we conclude that liquid crystals are not aligned by the surface morphology deformation of alignment layer after plasma alignment process.

In order to compare plasma alignment, we also observed the surfaces of alignment layer for rubbing alignment. Fig. 4-3 shows the surface morphology of rubbed polyimide. In this figure, we found that the grooves were produced on the alignment layer after rubbing treatment, i.e. the surface morphology of alignment layer experiences “directional” deformation. The strength of directional deformation of morphology can be defined by measuring optical retardation of alignment layer. However, according to the Ref [38], rubbed polystyrene and polycarbonate could not align liquid crystal even though they had optical retardation after rubbing. We concluded that although the grooves are produced on the alignment layer after rubbing, LC can not align only by the directional deformation; the interaction between LC molecules and polymers on the alignment surface is more important in rubbing alignment.

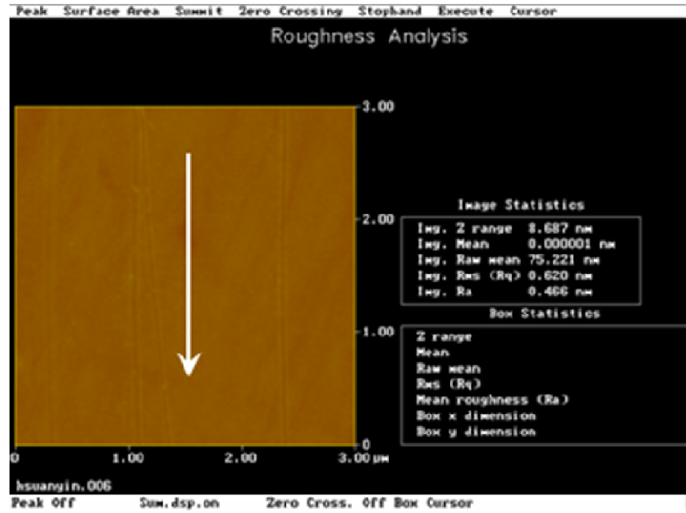

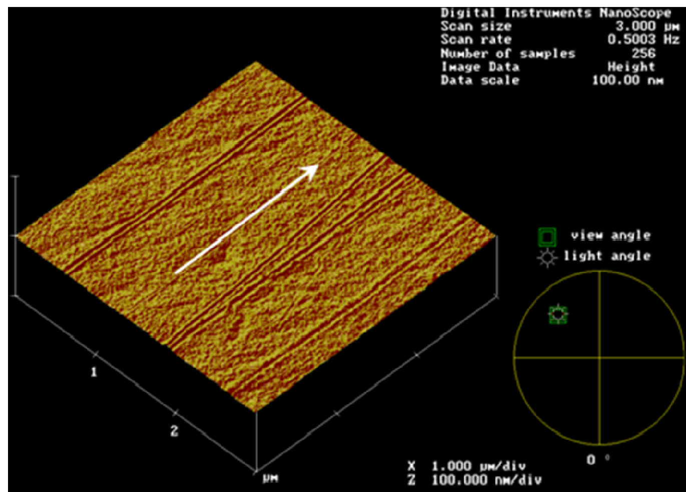

Fig. 4-3 Surface morphology of rubbed polyimide

4.2.2 V-T Characteristics

In this section, we will investigate the effect of plasma alignment on the V-T characteristics of TN cells, and compare with rubbing alignment. Fig. 4-4 shows the V-T characteristics of plasma-aligned TN cell with different incident angle of plasma. The parameters of alignment process were set as Table. 3-1 except the incident angle of plasma. The incident angle was defined as the angle between the direction of plasma and the surface normal. In Fig. 4-4, when the incident angle was 10°, the V-T curve was very unstable and have no obvious contrast between bright and dark state due to LC were not well-aligned on the alignment layer. With increasing the incident angle, the contrast ratio increases gradually owing to better dark state. Because the contrast ratio of a LC cell is affected directly by the LC alignment capability of alignment layer, we can conclude that better LC alignment capability is produced with higher incident angle.

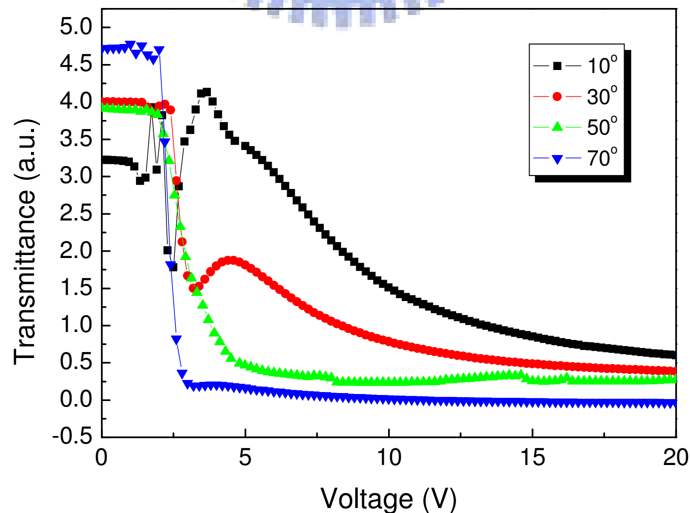

Fig. 4-4 V-T characteristics of plasma-aligned TN cell with different incident angle of plasma

When the incident angle was small, plasma bombarded on the alignment layer nearly perpendicular. The anisotropic deformation was not produced obviously in this case, which results in poor alignment capability. If the incident angle was large enough, i.e. the plasma is obliquely incident on the alignment layer, then larger anisotropic deformation was produced and made LC align. From Fig. 4-1, there did not exist "anisotropic deformation" on surface morphology. So this anisotropic deformation must occur on the chemical structure, which forces LC align in desired direction.

Next, we fixed the incident angle at 70°, and changed the scan times of plasma. Fig. 4-5 shows the V-T characteristics of TN cells of alignment layers treated by different plasma scan times. From the V-T curve of scan one time, the alignment layer could align LC. But due to insufficient alignment capability, there was severe light leakage at the dark state in the V-T curve of plasma scan one time. After scan five times, the light leakage had been decreased. The curve of plasma scan ten times is very similar to which scan five times because the alignment capability was saturated after plasma scan five times.

We want to find if the alignment capability of rubbing will also saturate. Fig. 4-6 shows the V-T characteristics of TN cells for different rotation rate of rubbing. Here we observed the results which were similar with plasma one. The TN cell of 50 rpm had poor bright state and light leakage at the dark state because the rotational rate was too slow to produce enough alignment capability. The cell of 200 rpm and 500 rpm had almost the same performance on V-T characteristic due to saturated treatment on the alignment layer.

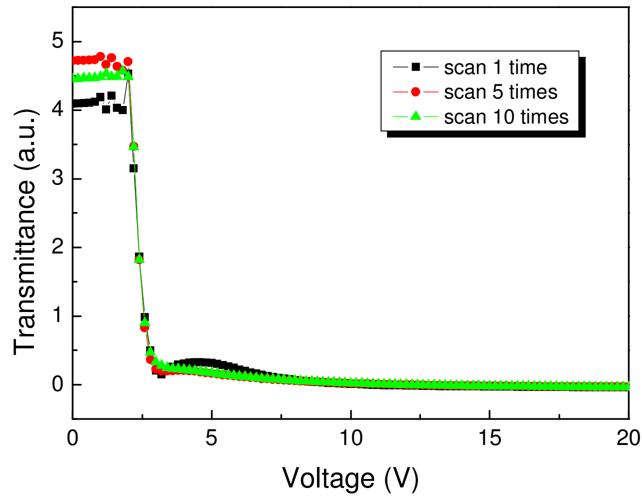

Fig. 4-5 V-T characteristics of TN cells treated by different plasma scan times

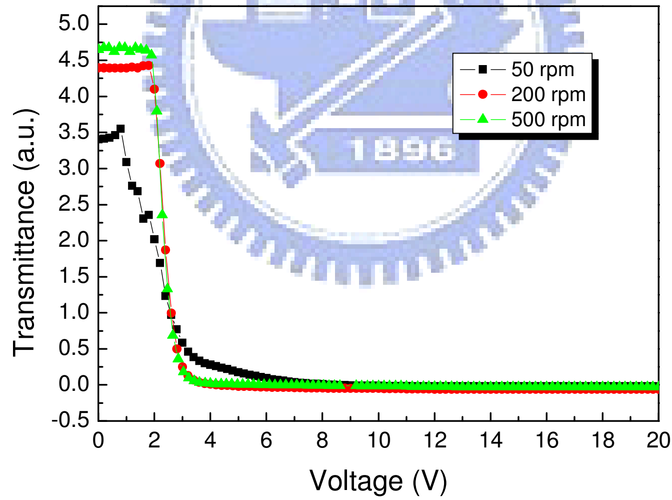

Fig. 4-6 V-T characteristics of TN cells for different rotation rate of rubbing

We also compare the V-T characteristics of rubbing aligned TN cells with plasma aligned one. We chose the two conditions of best performances of them. Fig. 4-7 shows V-T characteristics of rubbed and plasma aligned TN cells. Comparing with the cell prepared by rubbing alignment process, the V-T characteristics of plasma treated TN cells had light leakage after 2.8 V, where normal TN cell has steady dark state after 3.4V. The light leakage might cause by the weak anchoring surface energy of plasma treatment surfaces. The weak anchoring energy will be the main point to be improved for the application of plasma alignment.

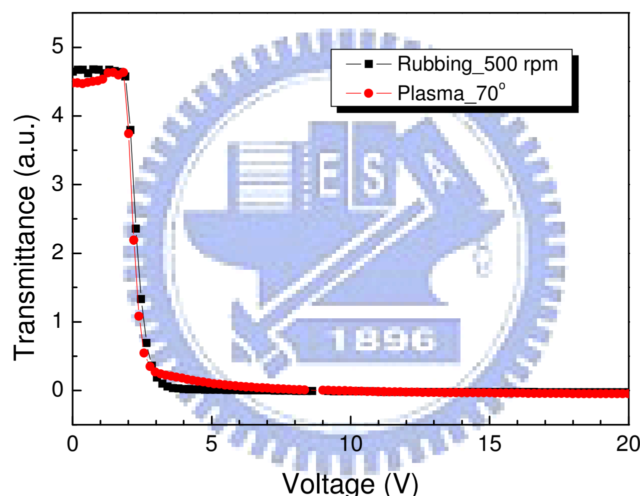

Fig. 4-7 V-T characteristics of rubbed and plasma aligned TN cells

4.2.3 NEXAFS Spectra

The mechanism of plasma alignment involves ion bombardment caused by unsymmetric or directional chemical bonds breaking. The Near-Edge X-ray Absorption Fine Structure (NEXAFS) spectroscopy was the best candidate to investigate the chemical bonding change of the alignment surface after plasma treatment.

The alignment direction is defined as y-axis, and the z-axis is defined normal to the substrate, as shown in Fig. 4-8. Both s- and p-polarization were used for the X-ray absorption measurement. The signal comes from the core-level excitation of chemical bond absorbing the X-ray energy and goes to molecular excited state. The absorption intensity is enhanced when the X-ray polarization is parallel to the orbital of chemical bond. The intensity of absorption is proportional to the amount of the specific chemical bonding.

The NEXAFS spectra of x and z axis of rubbed PI and plasma treated PI alignment were shown in Fig. 4-9 (a) and (b). The relationship of each peaks and bonds were also marked in the figure. It was found that all chemical bonds of alignment layer were damaged significantly after Ar plasma treatment, especially the carbonyl group normal to the substrate. The data indicated that the carbonyl group and polymer molecules in z-axis was severe damaged than in x-axis by the bombardment of plasma beams incident angle at 70° respective to the normal. Consequently, the elimination of polar groups, such as carbonyl group, significant weakened the interactions between LC molecules and alignment surface. Even though the asymmetry bond breaking helped the LC alignment, the reduction of polar anchoring energy may affect the electric-optic properties as shown in Fig. 4-7. As a result, the lost of polar group will be the fatal weakness for the application of plasma alignment technique.

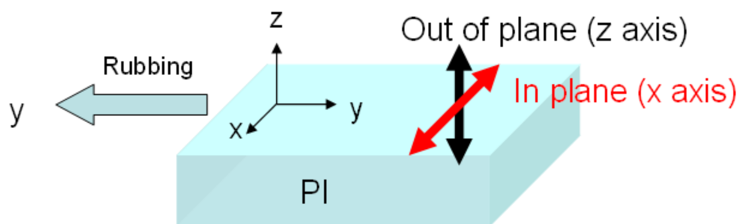

Fig. 4-8 The diagram of NEXAFS measurement

(a)

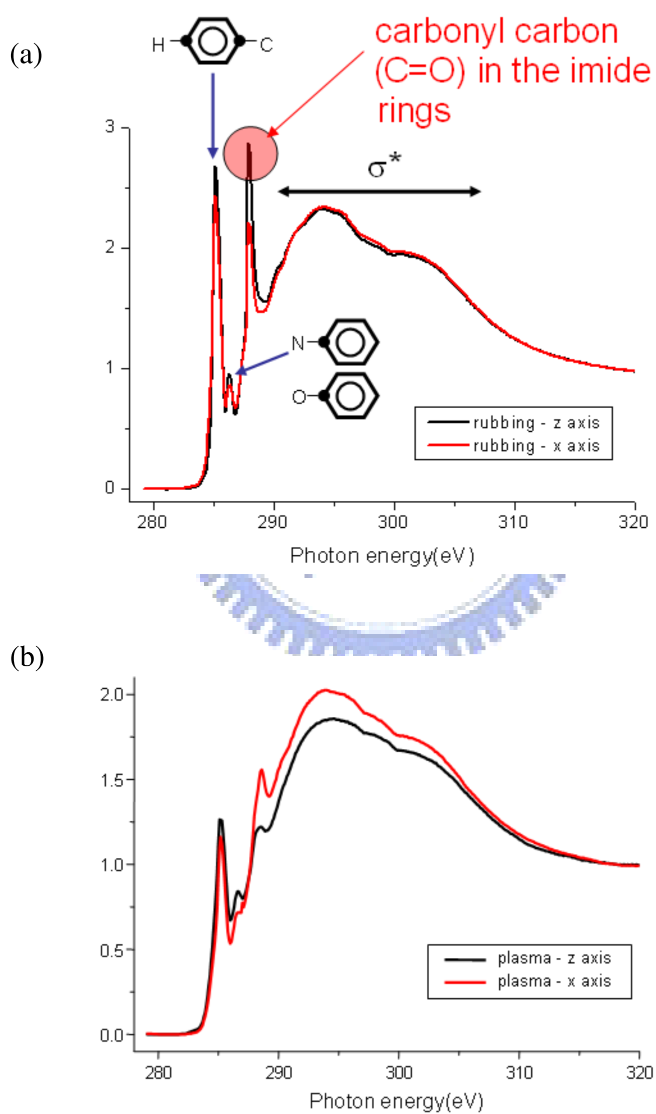

(b)

Fig. 4-9 NEXAFS spectra of x and z axis of

(a) rubbed PI surface (b) plasma treated PI surface

The NEXAFS spectra of x and y axis of rubbed PI and plasma treated PI alignment were shown in Fig. 4-10 (a) and (b). From this figure, the in-plane chemical structures of plasma aligned PI were also damaged severely than rubbing aligned one. Moreover, the directional change of in-plane chemical bonds was produced on the surface of the alignment layer for both rubbing and plasma alignment. Although both the difference between x and y axis were small, it was enough to align liquid crystal on the alignment layer.

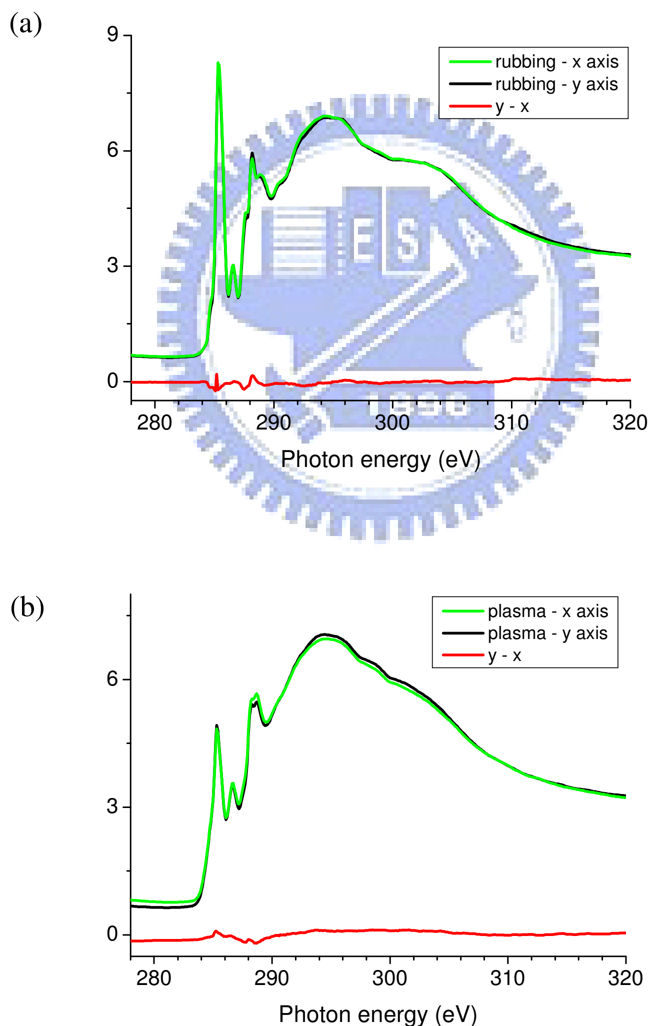

Fig. 4-10 NEXAFS spectra of x and y axis of

(a) rubbed PI surface (b) plasma treated PI surface

4.3 V-T characteristics of oxygen treated TN cells

According to NEXAFS data, the chemical bonds were damaged seriously after Ar plasma bombardment, especially the carbonyl bonds out of the alignment layer. The loss of polar functional group may cause the reduction of polar anchoring energy, and then affect the V-T characteristics of plasma aligned cell. Therefore, we would like to repair the carbonyl bonds to improve the performance of plasma alignment by introducing a new alignment process. Table. 4-1 shows the parameters of new plasma alignment process. As we can see, the oxygen plasma post-treatment was added after Ar plasma treated on the alignment layer. The assumption is to increase or repair the C-O bonding in z-axis on the PI surface, which may enhance the polar anchoring energy.

Table.4-1 The parameters of new plasma alignment process

Mode	Scan mode	Working gas 2	O_2
Voltage	450 V	Gas flow rate	20 sccm
Incident angle	70°	Scan times	5
Working pressure	0.2 mtorr	Scan velocity	10 mm/s
Working gas 1	Ar	Working gas 3	H_2
Gas flow rate	20 sccm	Gas flow rate	20 sccm
Scan times	5	Scan times	1
Scan velocity	10 mm/s	Scan velocity	5 mm/s

The electric-optic property of oxygen post-treatment cell was shown in Fig. 4-11. Compared to the one without oxygen treatment, the light leakage at dark state has been suppressed for the cell with oxygen treatment. The dark state of oxygen treated cell is even comparable with the rubbed PI one. As a result, the contrast of plasma alignment was able to increase by the oxygen after-treatment.

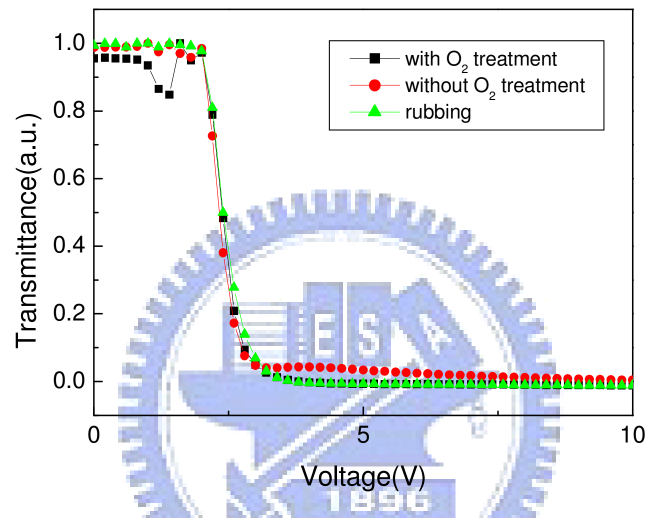

Fig. 4-11 V-T characteristics of oxygen post-treatment TN cell

4.4 Pretilt angle dependence

The operation of liquid crystal display requires monodomain alignment and control of pretilt angle of LC molecules on the substrate surface. The pretilt angle prevents the creation of reverse tilted disclinations in twisted nematic LCD. Furthermore, pretilt angle plays a very important role and also influence the LC alignment stability and electro-optical (EO) characteristics of LC operation modes using polyimide thin films. Fig. 4-12 shows the pretilt angle dependence as function of plasma scan times (one time, five times, ten times). The 1.85° pretilt angle

appeared only after scaning one time of plasma beam. The pretilt angle increases gradually after scan one time and 2.25° of pretilt angle is revealed after scan ten times. However, in the case of pristine polyimide thin films, the pretilt angle does not exist. It believes that scan times of plasma beam is the main factor in generating a LC pretilt angle.

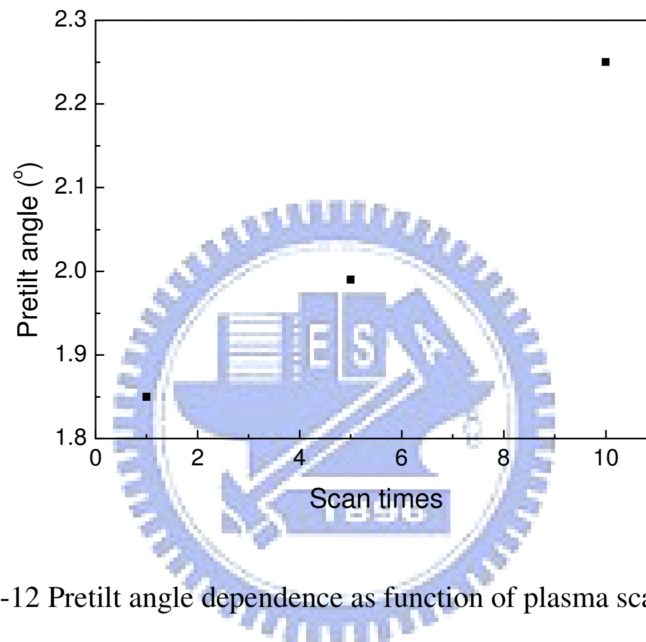

Fig. 4-12 Pretilt angle dependence as function of plasma scan times

After we introduced the oxygen plasma post-treatment right behind the original Ar plasma alignment process, the pretilt angle dependence was also observed. Fig. 4-13 shows the pretilt angle dependence as function of oxygen plasma scan times. The 2.11° pretilt was revealed after oxygen plasma scan one time. The pretilt angle decreased linearly with increasing oxygen plasma scan times. The pretilt angle became 1.34° after oxygen plasma scan five times.

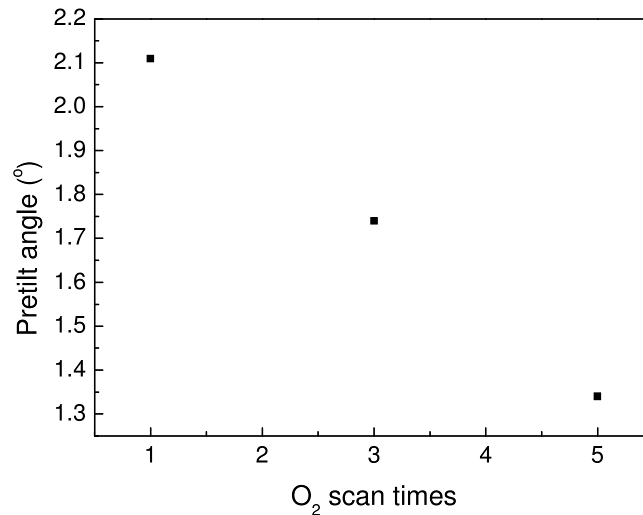

Fig. 4-13 Pretilt angle dependence as function of oxygen plasma scan times

4.5 Anchoring Energy dependence

The physical property of the boundary between alignment layer and liquid crystal has large influence to the performances of display, such as threshold voltage, operating voltage, transmittance, contrast, viewing angle...etc. Anchoring energy is one of important factors that directly affect the electro-optic properties. We had measured the polar anchoring energy dependence of rubbing alignment by high electric field method and capacitance measurement, and tried to compare with the V-T curve of rubbed TN cell.

Patterned ITO glass was used for substrate in anchoring energy measurement. The area of electrode was 1 cm^2. Rubbing alignment was chose to be the alignment method. The alignment direction of two substrate was anti-parallel, and the cell gap was about 30 μm. Here we compare the polar anchoring energy of different rotational rate in rubbing process.

4.5.1 High Electric Field Method

Fig. 4-14 (a) and (b) show the retardation dependence of rotational rate 500 rpm and 50 rpm using high electric field method. The fitting results are also shown in these figures.

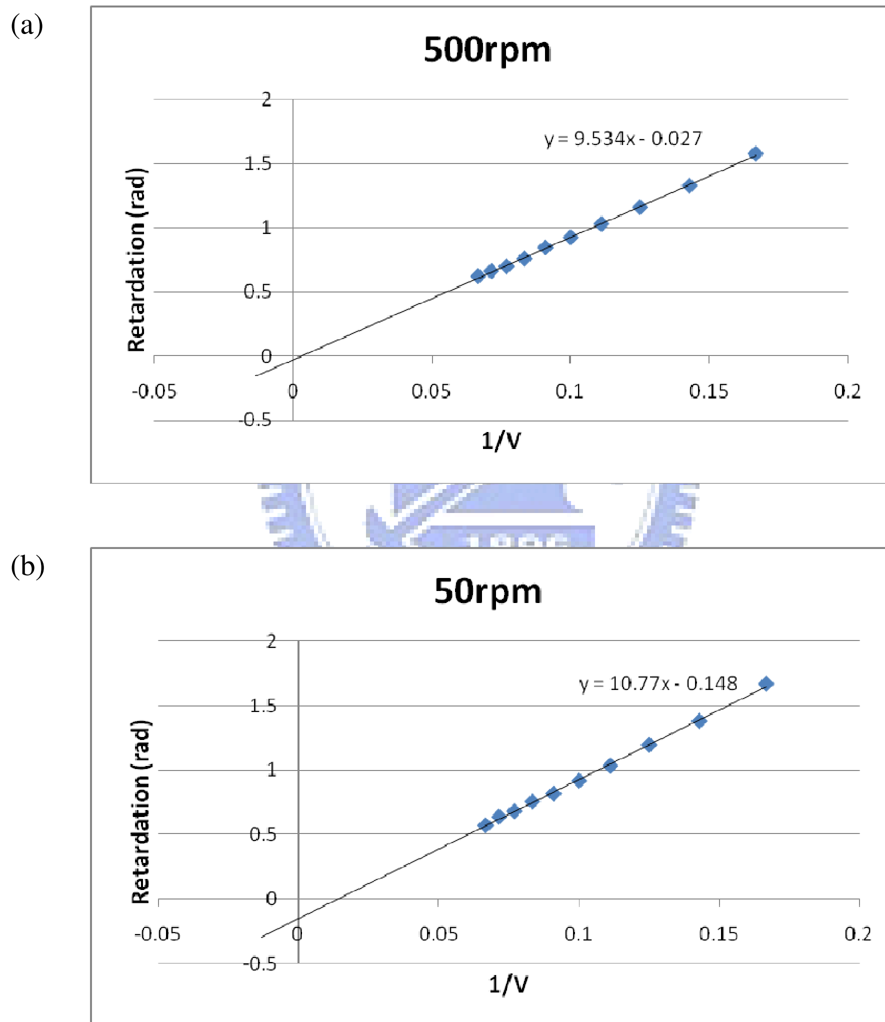

Fig. 4-14 Retardation dependence of rotational rate (a) 500 rpm and (b) 50 rpm

According to Eq. (3-11), the intercept at y-axis gives the anchoring energy. After calculation, the anchoring energies of rotational rate 500 and 50 rpm were 2.66×10^{-3} J/m^2 and 4.97×10^{-4} J/m^2 respectively. The polar anchoring energy of 50 rpm was much weaker than 500 rpm. Combining the V-T curves of different rotational rate (Fig. 4-7), we conclude that weaker anchoring energy will results in poorer electro-optic property, and the strength of anchoring energy depends on different alignment condition.

4.5.2 Capacitance Measurement

Fig. 4-15 and Fig. 4-16 show the capacitance dependence of rotational rate 500 rpm and 50 rpm using capacitance measurement method.

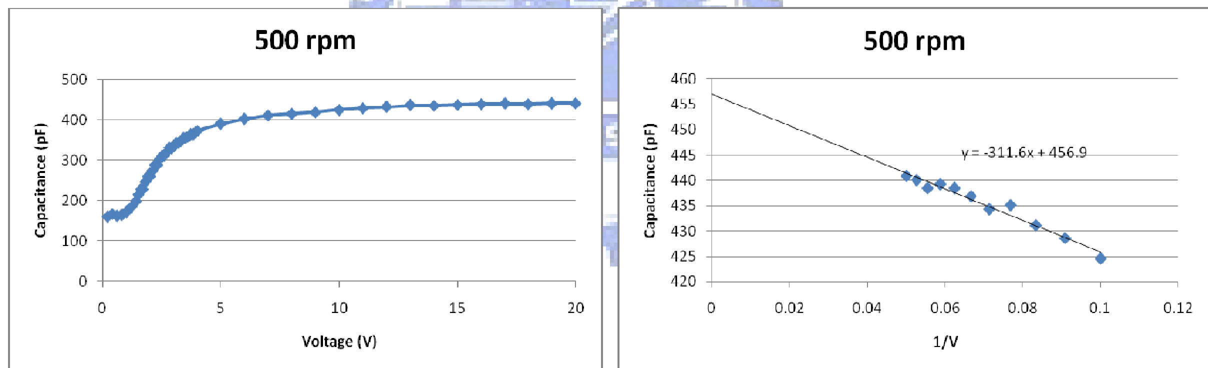

Fig. 4-15 Capacitance dependence of rotational rate 500 rpm

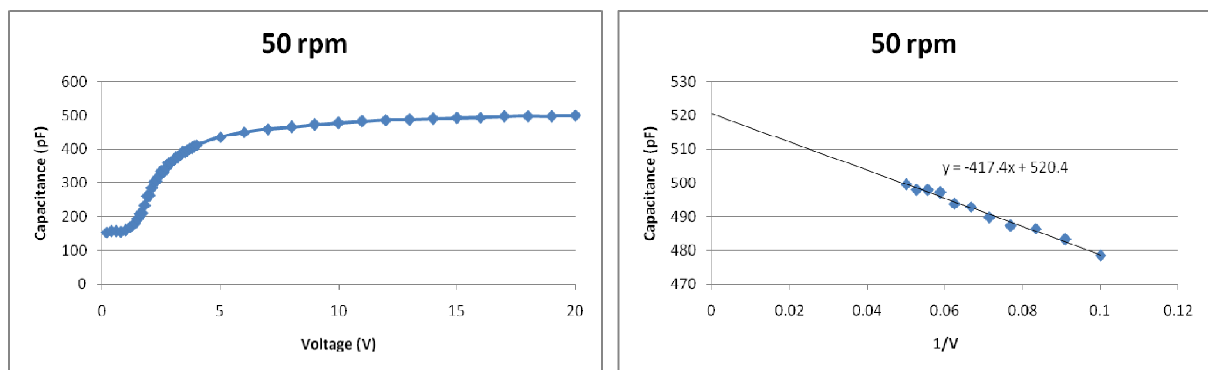

Fig. 4-16 Capacitance dependence of rotational rate 50 rpm

$C_{\perp}$, $C_{//}$ and $C_{\inf}$ could be obtained from Fig. 4-15 and Fig. 4-16. The value of capacitances and polar anchoring energy calculating from Eq. (3-15) were shown in Table. 4-2. From Table. 4-2, we found that the polar anchoring energy of 500 rpm and 50 rpm had the same order in magnitude. As we know, the V-T curve of 50 rpm in Fig. 4-7 had poorer performance than 500 rpm. In our prediction, the poor performance of the V-T curve might result from weak anchoring energy. But the polar anchoring energy of 50 rpm was even little larger than 500 rpm.

Table. 4-2 Parameters of capacitance measurement

	V_{th}(V)	$C_{\perp}$ (pF)	$C_{//}$ (pF)	C_{inf} (pF)	S (m^2)	W (J/m^2)
500 rpm	0.84	164	440.8	456.9	0.0001	1.90×10^{-5}
50 rpm	0.88	153	499.5	520.4	0.0001	3.07×10^{-5}

The comparison of polar anchoring energy by using high electric field method and capacitance measurement was shown in Table. 4-3. The magnitude of anchoring energy of 500 rpm and 50 rpm have difference of an order by using high electric field method, while the capacitance measurement doesn't have large difference. The results mean that the capacitance measurement might not be a suitable method for measuring polar anchoring energy.

Table. 4-3 Polar anchoring energy of different rotational rate in rubbing alignment

Anchoring energy (J/m^2)	500 rpm	50 rpm
High electric field method	2.66×10^{-3}	4.97×10^{-4}
Capacitance measurement	1.90×10^{-5}	3.07×10^{-5}

Chapter 5

Conclusions and Future Works

5.1 Conclusions

In contrast to current rubbing manufacturing process, the plasma alignment has fewer problems of electrostatic charge and debris and is the potential candidate to replace conventional rubbing process for the next generation large display. The TN (twisted nematic) mode LC is known for its easy fabrication and low driving voltage. However, rubbing is still the main alignment method for TN. In addition, the electro-optical characteristics, pretilt angle of TN cells and surface morphology of alignment layer after plasma treatment were investigated. The influence of TN cells between these two aligning methods was also be discussed.

During plasma alignment proceeds, the ions bombard on the alignment layer company with the etching effect. If the plasma is obliquely incident on the alignment layer surface, the anisotropic deformation will be produced, and then use this anisotropy to align liquid crystal. But by observing the AFM image of surface morphology, we did not find any directional deformation of morphology after plasma alignment. As a result, the anisotropy produced by plasma alignment should be the directional change of chemical structure, such as bond breaking. The phenomenon was observed from NEXAFS.

From V-T characteristics of TN cells, larger incident angle of plasma would get better performance of V-T characteristic, because the larger anisotropic change was

produced. By changing scan times of plasma, we found that the alignment capability was saturated after plasma scan five times, so the V-T characteristic of scan ten times was similar to which scan five times. Compare with the TN cell of rubbing, the V-T characteristic of plasma alignment had light leakage at the dark state, especially at the low voltage region of dark state. The light leakage might be caused by weak anchoring energy of plasma alignment. Therefore, improving the anchoring energy of plasma alignment is the most important issue for applications.

From NEXAFS data, the chemical bonds were damaged severely after plasma alignment, especially the carbonyl bond normal to the alignment layer. We suggested that the lack of carbonyl bond resulted in weak polar anchoring energy of alignment layer, and affected the V-T characteristic of plasma alignment. We hoped to repair the broken carbonyl bond normal to the alignment layer, and introduced oxygen post-treatment after Ar plasma alignment process. After the oxygen treatment, the light leakage of plasma alignment had been eliminated, and the performance could even compete with the rubbing one. We also observed pretilt angle dependence of Ar and oxygen plasma scan times. The pretilt angle increased with increasing Ar plasma scan times, but decreased with increasing oxygen plasma scan times.

The polar anchoring energy of different rotational rate in rubbing alignment had been obtained by using high electric field method. The anchoring energy of 50 rpm was much weaker than the one of 500 rpm. Comparing with the V-T curve of these conditions, we found that weaker polar anchoring energy will result in poorer performance of V-T curve.

5.2 Future Works

The electro-optical properties of TN cell, pretilt angle and surface morphology of plasma alignment were already discussed. Moreover, the characteristics of anchoring energy after original plasma alignment and oxygen post-treatment will be investigated. The NEXAFS spectra of oxygen post-treatment will also be measured. Furthermore, the alignment mechanism of plasma treatment is also important factor that need to be studied. The relationship between E-O properties and the alignment mechanism will also be discussed.

Reference

[1] M. Katayama, *Japan Display '89. Proc. 9th IDRC*, p.6 (1989).

[2] T. Uchida, T. Nakayama, T. Miyashita and T. Ishinaba, *Asia Display' 95, Proc. 15th IDRC*, p.599 (1995).

[3] M. Kubo, Y. Narutaki, S. Fujioka, Y. Maruyama, T. Shimada, Y. Yoshimura, M. Katayama, Y. Ishii, S. Yamakawa and A. Ban, U.S. patent 6295109 B1 (2001).

[4] D. K. Yang and J. W. Doane, *SID Symp. Digest Tech. Papers*, **23**, 759 (1992).

[5] Po-Chi Yeh and Claire Gu, "Optics of Liquid Crystal Displays", John Wiley, New York, 1999.

[6] Z. M. Sun, J. M. Engels, I. Dozov and G. Durand, J. Phys. II France, **4**, 59 (1994).

[7] J. Stohr, M. G. Samant, J. Luning, et al., Science, **292**, p.2299 (2001).

[8] P. Chaudhari, J. A. Lacey, S. C. A. Line and J. L. Speidell, Jpn. J. Appl. Phys., **37**, p.L55 (1998).

[9] C. Y. Lee, P. C. Liu, C. W. Chen, H. C. Tang, S. Lin, Y. Chang, W. T. Hsien, Y. J. Shih, J. M. Chen and C. D. Lee, *IDW 05*, LCT p2-2 (2005).

[10] C. Y. Lee, H. C. Tang, C. W. Chen, Y. J. Shih, C. H. Liu, C. H. Lin, K. H. Yang, S. H. Lin and H. C. Chang, *IMID 06*, p-26 (2006).

[11] W. Gibbons, P. Shannon, S. Sun and B. Swetlin, Nature, **351**, 49 (1991).

[12] M. Hasegawa and Y. Taira, *Proc. 14th IDRC*, p.213 (1994).

[13] Y. Kawanishi, T. Takimiya and K. Ichimura, Polym. Mater. Sci. Eng., **66**, 263 (1992).

[14] T. Yoshida, T. Tanaka, J. Ogura, H. Wakai and H. Aoki, *SID'97 Digest*, p.841 (1997).

[15] G. James and R. S. Lowder, Phys. Fluid, **9**, 1115 (1966).

[16] Z. M. Sun, J. M. Engels, I. Dozov and G. Durand, J. Phys. Ⅱ France, **4**, 59 (1994).

[17] P. Chaudhari, J. A. Lacey, S. C. A. Line and J. L. Speidell, Jpn. J. Appl. Phys., **37**, p.L55 (1998).

[18] P. Chaudhari et al., Nature, **411**, p.56 (2001).

[19] K. Eichhorn, K. J. Simon, F. Pleul, D. Janke and G. Gerlach, Surface and Coating Technology, **139**, p.257 (2001).

[20] H. Dong and T. Bell, Surface and Coating Technology, **111**, p.29 (1999).

[21] J. Stohr, M. G. Samant, J. Luning, et al., Science, **292**, p.2299 (2001).

[22] J. E. Fulghum, L. Su, K. Artyushkova, J. L. West and Y. Reznikov, Mol. Cryst. Liq. Cryst., **412**, p.361 (2004).

[23] C. Polhemus, Appl. Opt. **12**, p.2071 (1973).

[24] Filip Bruyneel, Herbert De Smet, Jan Vanfleteren and Andre Van Calster, Opt. Eng. **40**, p.259 (2001).

[25] T. J. Scheffer and J. Nehring, J. Appl. Phys, **48**, p.1783 (1977).

[26] G. Binnig, C. F. Quate, Phys. Rev. Lett., **56**, p.930 (1986).

[27] J. Stohr, NEXAFS spectroscopy, Springer-Verlag, New-York, 1996.

[28] S.unther, B. Kaulich, L, Gregoratti and Kiskinova, Progress in Surface Science, **70**, p.187 (2002).

[29] 許瑤真，魏德新，科儀新知第二十六卷第六期，p.8 (2005).

[30] Chao-Huang Chen, Y. J. Hsu, H. F. Hsiao, et al, *Proc. 8th Int. Conf. X-ray Microscopy*, p.285.

[31] Takahiro Sakai, Ken Ishikawa, Hideo Takezoe, et al, J. Phys. Chem. *B*, **105**, p.9191 (2001).

[32] D. F. Gu, Serif URAN and C. Rosenblatt, Liquid Crystals, **19**, p.427 (1995).

[33] K. H. Yang and C. Rosenblatt, Appl. Phys. Lett, **43**, p.62 (1983).

[34] H. Yokoyama and H. A. van Sprang, J. Appl. Phys, **57**, p.4520 (1985).

[35] Y. A. Nastishin and R. D. Polak, et al., J. Appl. Phys, **86**, p.4199 (1999).

[36] A. Murauski and V. Chigrinov, et al., Phys. Rev. E., **71**, 061707 (2005)

[37] Y. A Nastishin, R. D. Polak, S. V. Shiyanovskii and O. D. Lavrentovich, Appl. Phys. Lett., **75**, 202 (1999)

[38] J. M. Geary and J. W. Goodby, et al., J. Appl. Phys, **62**, p.4100 (1987).